SOLAR RADIO BURST TYPE II AND III WITH HALF WAVE DIPOLE ANTENNA

FARAH AQILAH MOHD PAUZI

FACULTY OF SCIENCE
UNIVERSITI MALAYA
KUALA LUMPUR

2020

SOLAR RADIO BURST TYPE II AND III WITH HALF WAVE DIPOLE ANTENNA

FARAH AQILAH MOHD PAUZI

THESIS SUBMITTED IN FULFILMENT OF THE REQUIREMENTS FOR THE DEGREE OF MASTER OF SCIENCE

DEPARTMENT OF PHYSICS
FACULTY OF SCIENCE
UNIVERSITI MALAYA
KUALA LUMPUR

2020

UNIVERSITI MALAYA

ORIGINAL LITERARY WORK DECLARATION

Name of Candidate: **FARAH AQILAH MOHD PAUZI**

Matric No: **SGR 150005**

Name of Degree: **MASTER OF SCIENCE**

Title of Thesis: **SOLAR RADIO BURST TYPE II AND III WITH HALF WAVE DIPOLE ANTENNA**

Field of Study: **EXPERIMENTAL PHYSICS**

I do solemnly and sincerely declare that:

(1) I am the sole author/writer of this Work;
(2) This Work is original;
(3) Any use of any work in which copyright exists was done by way of fair dealing and for permitted purposes and any excerpt or extract from, or reference to or reproduction of any copyright work has been disclosed expressly and sufficiently and the title of the Work and its authorship have been acknowledged in this Work;
(4) I do not have any actual knowledge nor do I ought reasonably to know that the making of this work constitutes an infringement of any copyright work;
(5) I hereby assign all and every rights in the copyright to this Work to the University of Malaya ("UM"), who henceforth shall be owner of the copyright in this Work and that any reproduction or use in any form or by any means whatsoever is prohibited without the written consent of UM having been first had and obtained;
(6) I am fully aware that if in the course of making this Work I have infringed any copyright whether intentionally or otherwise, I may be subject to legal action or any other action as may be determined by UM.

Candidate's Signature Date:

Subscribed and solemnly declared before,

Witness's Signature Date:

Name:

Designation:

SOLAR RADIO BURST TYPE II AND III WITH HALF WAVE DIPOLE ANTENNA

ABSTRACT

An investigation into the physics of solar radio burst type II was done to understand the frequency gap between its fundamental and harmonic emissions that happen as aftershocks of Coronal Mass Ejection (CME). Up until now, the evolution of type II and its associated coronal wave still remain a mystery. Hazardous CME study upholds its fore coming danger to human and technology. This work also addresses the issue of the lack of spatial resolution of previous solar radio burst type II studies. An instrument produced by ETH Zürich namely the *Compound Astronomical Low-cost Low-frequency Instrument for Spectroscopy and Transportable Spectrometers* (CALLISTO) was used. A newly designed low frequency antenna array produced through a collaboration between University of Malaya (UM) and the Yunnan Astronomical Observatory (YNAO) of China named the *Half Wave Dipole Antenna* (HWDA) array is also used in this research. This dissertation describes the newly designed proposed instrument and its significance in studying solar radio burst type II. Comparison study is also made with other leading radio solar monitoring instruments such as the CALLISTO, *Chinese Spectral Radio Heliograph* (CSRH) and *Murchison Widefield Array* (MWA). Upon setting up the HWDA, the radio frequency interference (RFI) of the observation site in UM is shown to emphasize the suitability of the selected candidate site. Furthermore, it also includes the optimal observation design and strategies for future detection. This dissertation shows the preliminary results of the proposed instrument by detecting solar radio burst type III confirmed by CALLISTO. The same event also indicates a correlation ratio of 0.94 with that coincides with solar flare class C 2.0. Gopalswamy power law and the electron density were used to estimate the density scale height (L_n). At the bandpass frequency of the HWDA L_n was found to be 1.41 x 10^8 m. The

calculated shock speeds are hence found to be 2.350 x 10^3 ms^{-1} and 1.504 x 10^7 ms^{-1} for low and high drift rates, respectively. These shock speed values indicate that the kilometric type II associated with CMEs are able to drive shocks only when it reaches far into the interplanetary medium.

Keywords: Astronomy, Astrophysics, Solar Physics, Radio Astronomy

LETUPAN SINARAN RADIO MATAHARI JENIS II DAN III MENGGUNAKAN ANTENNA DWI-KUTUB SEPARA GELOMBANG

ABSTRAK

Siasatan terhadap fizik letupan sinaran radio matahari jenis II telah dilakukan untuk memahami jurang frekuensi antara pancaran asas dan harmonik yang berlaku kerana penyangkalan Kumpulan Pelemparan Korona (CME). Sehingga kini, evolusi untuk jenis II dan gelombang korona yang berkait dengannya masih kekal sebuah misteri. CME berisiko perlu dikaji untuk menyiasat tahap bahaya kepada manusia dan teknologi. Kerja ini juga menangani isu kekurangan resolusi gambaran struktur letupan sinaran radio matahari jenis II dari kajian terdahulu. Sebuah alatan kajian yang dihasilkan oleh ETH Zürich iaitu *Alat Kompaun Astronomi Kos-rendah Frekuensi-rendah untuk Spektroskopi dan Spektrometer mudah alih* (CALLISTO) telah digunakan. Sebuah tatajalur antenna berfrekuensi rendah baru direka melalui hasil kerjasama antara Universiti Malaya (UM) dan Balai Cerap Astronomi Yunnan (YNAO) China yang dinamakan *Antenna Dwi-kutub Separa Gelombang* (HWDA) juga digunakan dalam kajian ini. Disertasi ini menerangkan peralatan yang direka itu dan kepentingannya dalam mengkaji letupan sinaran radio matahari jenis II. Perbandingan antara alat pemantauan sinaran radio matahari terkemuka lain seperti CALLISTO, *Spektrum Radio Heliograf Cina* (CSRH) dan *Tatajalur Medan kajian luas Murchison* (MWA) juga dibuat. Dalam pembinaan HWDA, semakan gangguan frekuensi radio (RFI) persekitaran UM dilakukan bagi menepati kesesuaian pemilihan tapak kawasan balai cerap. Selain itu, ciri pemerhatian yang optimum dan strategi untuk pengesanan masa hadapan juga diselidik. Disertasi ini juga menunjukkan keputusan pertama peralatan terkini itu dengan mengesan letupan sinaran radio matahari jenis III yang disahkan oleh CALLISTO. Peristiwa sama juga menunjukkan nisbah korelasi 0.94 dengan yang bertepatan dengan suar suria kelas C 2.0. Model gandaan Gopalswamy dan

ketumpatan elektron digunakan untuk menganggar ketinggian skala ketumpatan (L_n). Pada frekuensi jalur pintasan HWDA L_n didapati 1.41 x 10^8 m. Dengan itu, kelajuan mengejut yang dikira adalah 2.350 x 10^3 ms^{-1} bagi kadar rendah tersasar dan 1.504 x 10^7 ms^{-1} bagi kadar tinggi tersasar. Nilai-nilai kelajuan mengejut tersebut menunjukkan bahawa kilometrik jenis II yang berkaitan dengan CME mampu meloncat apabila ia sampai jauh ke dalam medium antara planet.

Kata kunci: Astronomi, Astro Fizik, Fizik Matahari, Astronomi Radio.

ACKNOWLEDGEMENTS

I would like to express my sincere gratitude to my supervisor, Associate Professor Dr. Zamri Zainal Abidin for his guidance and wisdom. His knowledge throughout this course was really helpful and I as a student will forever be in debt for his knowledge sharing.

I would like to thank my family. My dad for supporting me in pursuing this degree although it is not a popular field in Malaysia. Even in battling cancer, he would asked about my thesis. My mom for being my idol, to never stop studying even when you're 50. My husband, upgraded friend who is also a circuit foremen and impromptu computer guy. My aunt for always taking care of my son, while mama goes to UM. Separation anxiety flew pleasantly under her care. Thank you as well to all other family members for being there for me.

Not forgetting my research group, from radio cosmology lab. Our sifu, Professor Dr. Zainol Abidin, for always suggesting ways to troubleshoot circuit error. My senior, Nabilah for always being my plus one throughout the course. My seniors, Suzyan, Shaiful and Zul for always lending their ears and frantic wisdom. My friend Ching Yee who always help me with python coding even during late nights. Other members as well for making the journey filled with rainbows.

Also thank you to all members of astronomy lab. Especially, Dr. Nazatulshima for providing us an observatory site. Involuntarily, some of her suggestions does help me a lot in my studies. Not forgetting, Yunnan Astronomy Observatory staff members. Dong Liang for constantly exchanging information and suggesting ways in doing research. Shao Jie for helping in constructing the antenna and sharing limitless knowledge on electromagnetism. Thank you for teaching me basics. Also, a hearty gratitude to Mr Christian Monstein, for creating e-Callisto.org making the solar radio burst data public and available online. Lastly, I am forever grateful for all the necessary encouragement.

TABLE OF CONTENTS

LIST OF FIGURES

LIST OF TABLES

LIST OF SYMBOLS AND ABBREVIATIONS

CALLISTO	:	Compound Astronomical Low-cost Low-frequency Instrument for Spectroscopy and Transportable Spectrometer
CSRH	:	Chinese Spectral Radio Heliograph
GOES	:	Geostationary Operational Environmental Satellite
HWDA	:	Half Wave Dipole Antenna
MWA		Murchison Widefield Array
UM	:	University of Malaya
VSWR	:	Voltage Standing Wave Ratio
YNAO	:	Yunnan Astronomical Observatory

LIST OF APPENDICES

CHAPTER 1: INTRODUCTION

1.1 Research Background

Nigh on everything on Earth evolved around the Sun. Biologically, we still react to sunset and sunrise. Before there were light and fire, the source of light was only sunlight and only full moon gives people sight at night. Crop plans were given clues through its movement and its concept throughout the year. People even worshipped and considered the Sun as a deity object. Solar astronomy began to widen since the discovery of heliocentric solar system. It was then philosophical astronomers discovered the concept of nuclear fusion and the generation of vast amounts of energy originated from the Sun. Solar radio astronomy is still facing unresolved spatial resolution capacity and the problem needs to be tackle by researchers. Large interferometry would implied in solving the problem partially. This would be discussed further in Section 2.

1.1.1 Solar atmosphere

The Sun have three atmospheres known as solar atmospheres which are the photosphere, the chromosphere and the corona. The photospehere is the first layer of the solar atmosphere just above the core (Layton & Freudenrich, 2000). Heat travels outside the atmosphere through absorption and reemission radiation transportation (Kundu, 1965). As heat travels, more radiation escapes accumulates and the concentration of radiation decreases as it progress to the outermost layer of the solar atmosphere. Most of travelling radiation came from the first layer with 300km thickness just above the core which is the photosphere is due to the radiation emission decreases with the increasing travelling distance furthered from the solar core (Kundu, 1965). The photosphere can be describes as granules that behave just like the bubbles of boiling water (Layton & Freudenrich, 2000). The heat via radiation transportation from the turbulent convection causing hot gasses movement leaving cold gases behind. This is living proof of convection zone existence which can be observe at the center of a large sunspot. At a very high magnitude of magnetic field, convection zone are being inhibit causing a certain region on the photosphere to have darker patch and usually they are no individual formation. The center of the sunspot is call umbra and just like the egg yolk, the white part are call penumbra (Kundu, 1965). Sunspots are shortlived events compared to the magnetic field itself (Kundu, 1965). Solar activities arises from high magnetic field region near sunspot groups. Appleton and Hey pioneered solar radio observation in 1946 while monitoring solar flares during the great sunspot group (Kundu, 1965).

The second layer of the solar atmosphere which the middle layer just above the photosphere is the chromosphere. At the chromosphere, there are many source that might be causing the high magnetic energy existence (Kundu, 1965). Transported hot and cold gases in the photosphere are causing shock wave that heats up the chromosphere in dispersing manner producing spike like tiny hot gases which is also known as spicules (Layton & Freudenrich, 2000). During an eclipse this spicules are visible and photograph may be captured (Kundu, 1965). Whereas for chromosphere, the image of the layer can be seen using a Hydrogen-alpha (Hα) light telescope (Layton & Freudenrich, 2000).

The last and third layer of the solar atmosphere is call the corona. Corona is a direct translation that defines a crown which can be observed during the solar eclipse and through a observe coronagraph (Layton & Freudenrich, 2000). A occurence known as the prominences can be seen as a bright arches on the solar surface when compared to interstellar space background or a dark filament on the solar surface itself existed at the corona that appears along the magnetic lines of a sunspot pairs (Kundu, 1965; Layton & Freudenrich, 2000). As the condensation of cool gas forms the bright arch appears along the magnetic lines, the prominences disappears gradually when a sudden magnetic field change caused by the shortliving formation of sunspot and the loop prominences is usually related to solar flares (Kundu, 1965). One of disastrous major event known as the coronal mass ejection (CME) occurs when the Sun ejects mass of particle and energies out of the solar surface. Until now, the association of AR and CME still remain as a debate among scientist and still remain active as on-going research eventhough AR is regarded as the origin of CME (Chen et al., 2011).

1.1.2 Solar Radio Burst

The discovery of Solar Radio Burst is known since 1942 (Kundu, 1965), to date it is remain as great unresolved mystery. In 1932, Jansky discovered the first radio observation from the Milky Way (Kundu, 1965). Since Jansky, many observed radio events have been observed by scientists globally especially in the Milky Way. Most of radio technology observations were developed from military purposes instruments which are modified technology that studies the interstellar space and cosmic radio (Kundu, 1965).

Solar Radio Burst occurs when the Sun emits energy in the radio frequency spectra out of the solar surface into the interstellar medium. It is a transient enhancements of solar radio emissions due to energies of accelerated electrons is greater than the quiet corona thermal energy (Klein et al., 2018). Till now, there are known five main types of Solar Radio Burst, Solar Radio Burst Type I, II, III, IV and V which is observed using a radio spectrogram. This spectrogram is a specialized two dimensional image that interprets radio spectrum with an orange-blue gradient color contours. The spectrogram is an image that represents a frequency against time graph. The orange-blue gradient is indicating the magnitude of solar radio burst intensity. Usually the an orange color represents higher intensity, while blue color indicate lower intensity but there are limitless option in setting the color contours gradient. These spectrograms can be obtained with *Compound Astronomical Low-cost Low-frequency Instrument for Spectroscopy and Transportable Spectrometers* (CALLISTO) technology.

Solar Radio Burst Type I is a noise storm with long hour series of short and narrow band that appears as continuously. Solar Radio Burst Type II have a tick marked shaped is a slow drift (Monstein, 2011). This name is based on its slow frequency drift. Frequency drift is simply a frequency difference divided by time difference. The usual unit for frequency drift is megahertz per second (MHz/s). Solar Radio Burst Type III is known as fast drift (Monstein, 2011) because it has fast frequency drift. For Solar Radio Burst Type III groups, they tend to have short duration that usually last in seconds to minutes. This occurrence are due to particles that arises from solar flare that accelerates electron in the corona with a really high velocity (Monstein, 2011). Solar Radio Burst Type IV is known as broad continuum spectrum. Usually the continuum appears just before Type I. The last type is Solar Radio Burst Type V. This type is a short lived continuum. In a spectrogram, Solar radio Burst Type V looks like a flag at the lower requency of Type III (Monstein, 2011).

1.1.3 Solar Flare

A complex sunspot group with a sudden change in their magnetic energies will cause violent explosion that can be observed in x-ray spectra called solar flares (Pekünlü, 1999; Layton & Freudenrich, 2000). Usually, a solar flare is a recurring event that may differ in form, brightness and spectrum at the same AR and it happens at the same chromospheric region. As a solar flare progress over time, when it reach the peak brightness a solar flare rapidly expand its border which are known to exhibit a "flash" phase that might explain the effects of distance filament at the sun surface are caused by hydrodynamic disturbances. Solar flares are just like sunspot, they too have short lifespan (Kundu, 1965). Solar flares are not CMEs. Chen et al. (2011), stated that there are two types of flares, confined and eruptive flares. There are three classes, C-class, M-class and X-class (Marusek, 2007). Plasma oscillation excitation in solar flares and CMEs cause radio energy to emit at the sun surface (Zucca et al., 2012). This type of radio emission is the known Solar Radio Burst. The solar flare can be studied using X-ray flux provided by Geostationary Operational Environmental Satellite (GOES).

1.1.4 CME

CME is a current event discovered in space studies in the early 1970s. It took nearly two decades for scientist to realize the importance of the event (Gopalswamy, 2016). The CME itself is a mystery. They are known as major natural hazard as it causes large solar energetic particles (SEP) and huge geomagnetic storm (Gopalswamy, 2016).

1.2 Problem Statement

Solar Radio Burst is an event that occurs at the sun surface. Up until now, the generation of type II still remain a mystery. The association of type II wave in the involvement of which coronal wave involved is still being studied (Zucca et al., 2012). There are two types of shock fronts which are known as blast shock and piston shock. In most cases, these shock fronts shows an appearance and motion that were accompanied by solar radio burst type II (Eselevich et al., 2016). Shock waves are disturbances that are faint at the nose of CME but strongly visible at the rear and flanks (Gopalswamy, 2016). The connection between the shock waves and solar radio burst type II, i.e. the splitting of the fundamental and harmonics emission, and its propagation, is usually related to CMEs. CME which is currently known as a major natural hazard acts as a root that causes severe weather in earth's space environment, which eventually pose danger to humans and their technology (Gopalswamy, 2016). The space weather is an important building block of CME, one of which is closely related to solar radio burst type II. Thus, studying the frequency gap gives more information on solar radio burst type II. Just like pixelated image, higher pixels show a clear image. There are existing technologies (i.e. CALLISTO) that currently active in investigating solar radio burst type II, but nonetheless they are not focusing at smaller range which happens at the frequency gap. In cases of short-lived solar radio burst type II, when it happens at similar times and frequencies of other radio signal, it is hard to identify the signal (Zucca et al., 2012). Thus, a more highly focus technology is needed to aid the investigation of solar radio burst type II frequency gap.

1.3 Research Objectives

1. To show the ability of detecting solar radio burst using the newly designed Half Wave Dipole Antenna (HWDA).
2. To identify the capability of HWDA by studying the relationship between solar radio burst and solar flare.
3. To discover the potential of HWDA in investigating solar radio burst through its distinct emissions, shock speed and drift rate.

The ability of detecting solar radio burst shows the reliability of the system in observing the radio signal of the sun. The half wave dipole antenna system pointed at every direction of north, east, west and south makes it an ideal system of detecting radio signal from the sun. The newly design system is the first to observe specifically at the range of 55 to 65 MHz. It has been optimized to measure solar radio burst within that range. Definitely, this is a new approach of observing solar radio burst.

As a new instrument, HWDA needs to be acknowledge scientifically through research. The science behind HWDA can be proven by studying the relationship between solar radio burst type and solar flare. Solar Radio Burst type III is caused by flare accelerated electron beams propagating through the corona at high velocity (Monstein, 2011). Undeniably the CME is a big disastrous event and the interplanetary shocks are steered by CME but most coronal shocks are driven by flares (Zucca et al., 2012). This circumstance has been related to the occurrence of solar radio burst in research community, one of them is solar radio burst type III in relation with solar flares.

The HWDA is a new platform in investigating solar radio burst. Solar radio burst type II in relation with coronal remains a mystery (Zucca et al., 2012). Previous study have shown the fundamental emission of Solar radio Burst type II lies between 20 and 60 MHz, while the harmonic emission tails at between 60 and 90 MHz (Zucca et al., 2012). From the scientific investigation, both of the emission coincides at approximately 60 MHz. Meanwhile, another research investigated that the harmonic emission of solar radio Burst Type II starts between 60 MHz and 300 MHz in the harmonic band (Vršnak & Lulić, 2000). By narrowing the frequency at approximately 60 MHz, the physical properties and the possible pattern at the frequency gap can be investigated. Moreover, an indistinct approximation of shock speed from the drift rate can estimate solar behavior.

1.4 Research Hypothesis

1. At low range of 55 to 65 MHz solar radio burst is detected with the new profound Half Wave Dipole Antenna technology.
2. The fitting of solar flare from Geostationary Operational Environmental Satellite (GOES) Xray Flux and solar radio burst type III from CALLISTO indicate an ideal comparison between the two events.
3. The Gopalswamy model can be used to estimate the shock speed of solar radio burst type II in gaining more information about the gaps between the fundamental and harmonic emission.

1.5 Significant of Research

This investigation is a novel research which uses new technology to study the solar radio burst. Eventually, the solar radio burst is compared to solar flares and coronal mass ejections (CME). Upon installation, the reliability of the technology is tested, ensuring it can detect solar radio burst. The idea of the new profound technology is to focus on solar radio burst type II by relating the separation between fundamental and harmonic emissions. This research presents novelty in which will focus on solar radio burst type II with flares and coronal mass ejections (CME), by relating the separation between fundamental and harmonic emissions. The construction of this new array is a result of a direct collaboration between University of Malaya and the Yunnan Astronomical Observatory (YNAO) of China.

1.6 Research Question

Why do people study Solar Radio Burst?

There are many reasons related to the investigation of Solar Radio Burst. These types of event that occur in the sun, can be used as an instrument for investigating acceleration processes that is responsible for high exciter velocities. Secondly, they can be used as a natural plasma probes traversing lots of information regarding to various space plasma parameters (Behlke, 2001).

CHAPTER 2: LITERATURE REVIEW

2.1 Solar Astronomy

The solar atmosphere consist of 3 layers which are the photosphere, the chromosphere and the corona. The photosphere in turn as the source of solar flares which create blasts of X-rays, ultraviolet radiation, electromagnetic radiation and radio waves, expands about hundred thousands of miles over the sun's surface have the temperature of around 10,000 degrees F (5,500 degrees C). While, the temperature can be as low as 7,300 degrees F (4,000 degrees C) at the umbra of big sunspots on the photosphere. As it progresses to the chromosphere the temperature drops at around 7,800 degrees F (4,320 degrees C). Then, it rose significantly in the solar corona. Surprisingly the corona can get shockingly hot from the rest of the Sun. The temperatures increase from 1.7 million degrees F (1 million degrees C) to in excess of 17 million F (10 million C). To date, the fluctuating temperature as it progresses from the photosphere to corona remains a cryptic puzzle (Kundu, 1965).

The heliosphere is a vast region of magnetic field and charged particles of the solar wind extended out of the Sun surface into the interstellar space. Solar wind are expansion of plasma out of the Sun's surface at a supersonic speed. Due to its supersonic speed, the high kinetic energy let the plasma particle to escape the Sun's gravity. The magnetic fields from the interstellar and the Sun doesn't mix form like an atmosphere that shields most of our solar system from galactic cosmic rays. Its outer edges where the solar wind interface with the interstellar medium is the heliopause. An elongated tail extended out of the heliosphere is called the heliotail (Bhatnagar & Livingston, 2005).

Biermann and Schwarzschild had proposed the photospheric granulation might generate chromosphere heating due to acoustic waves' energy dissipation, through shock waves as the energy dissipate in heating the chromosphere and corona (Bhatnagar & Livingston, 2005). Shock waves are immediate discontinuous changes of plasma in density and pressure at supersonic speed (Bhatnagar & Livingston, 2005).

The Sun is a giant ball of rotating gas does not rotate uniformly. This is creating differential in solar rotation thus be the source of solar dynamo. Scheiner find that the sun does not rotate like a solid body (Bhatnagar & Livingston, 2005). Such that the equator completes one rotation in 27 days and the pole in 31 days (Bhatnagar & Livingston, 2005). Solar dynamo is the generation of sunspot through interaction of convection, turbulence, differential rotation and magnetic fields.

2.2 Lack of Spatial (Focus) on Solar Radio Burst Type II Gap

Solar radio burst type II is usually related with flares and CMEs has two emissions, namely fundamental and harmonic emission. Up until now, there is no direct resolution on the gap between the fundamental and harmonic emission. For Solar Radio Burst type II, in 2012, Zucca et. al. has stated the fundamental emission is seen at 20 and 60 MHz. At harmonic emission the harmonic backbone of the solar radio burst type II lies between 60 to 90MHz (Zucca et al., 2012). Therefore, the fundamental and harmonic emission may split at the frequency of about 60 MHz. This is which a process in tackling the unresolved spatial resolution.

An investigation by Zimovets et al. (2012), illustrate a model which provides the basis for the frequency gap study, via the newly constructed Half Wave Dipole Antenna array. They have studied an event specifically for frequency splitting in harmonic emission where they divided into two frequency components.

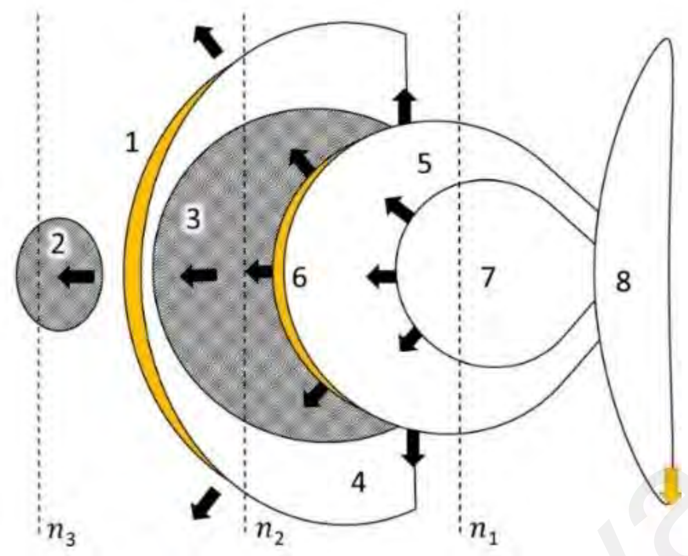

Figure 2.1: Schematic illustration of eruptive events on November 3rd, 2010.

Figure 2.1 shows a schematic illustration of the eruptive event on the 3rd November 2010, where the yellow arrow indicates direction to the earth. Figure 2.1 is describing the solar atmosphere kinematics by associating solar radio burst with other eruptive solar events. The Zimovets model is a study that investigate Solar Radio Burst Type II especially in the harmonic emission. In Figure 2.1, the numbers indicate; (1) hypothetical shock wave, (2) lower frequency component (LFC) harmonic emission source of solar radio burst type II, (3) higher frequency component (HFC) harmonic emission source, (4) turbulent magnetosheath, (5) warm plasma rim with its (6) upper (leading) edge, (7) hot erupting plasma rope and (8) the photosphere (Zimovets et al., 2012). The shaded region represents the harmonic emission. Based on the Figure 2.1, the harmonic emission is divide into two components that represents the higher frequency, HFC and lower frequency, LFC. The motion of the events are represent using the black arrows and their lengths proportionate to the velocities. Zimovet assumed the constancy of the background electron plasma concentration levels. Gravitational stratification is marked with black dashed lines. n represents the plasma density with $n_1 > n_2 > n_3$.

2.2.1 Magnetic Reconnection and MHD waves

The origin of Solar Radio Burst Type II is postulated through a pressure pulse mechanism using magnetic reconnection equation which produce Magnetohydrodynamic (MHD) blast waves (Vršnak & Lulić, 2000). The equation describes the movement of plasma out of the sun surface. It also indicates the magnetic field movement in the Solar Radio Burst which is a component of electromagnetic wave. The magnetic reconnection equation can be derive using Maxwell relation and the Ohm's Law. The Maxwell relation,

$$\nabla \times \boldsymbol{E} = \frac{\delta \boldsymbol{B}}{\delta t}$$

$$\nabla \times \boldsymbol{B} = \mu_0 J$$

$$\nabla \bullet \boldsymbol{B} = 0$$

The Ohm's law,

$$J = \sigma \boldsymbol{E}$$

The magnetic reconnection equation,

$$\frac{\delta \boldsymbol{B}}{\delta t} = \nabla \times (\boldsymbol{v} \times \boldsymbol{B}) + \frac{1}{\mu_0 \sigma} \nabla^2 \boldsymbol{B}$$

(Fitzpatrick, 2014)

$\boldsymbol{E}$ is the electric field, J is the current per area, $\boldsymbol{B}$ is the magnetic field, $\boldsymbol{v}$ is the velocity of the plasma particle (wave), μ_0 is the magnetic constant and σ is the plasma conductivity. The whole equation is the summation of convection term and diffusion term which can be represent simply by first and second term respectively (Fitzpatrick, 2014). At a very high conductivity, the second term (diffusion term) is approximated zero, the derivative of magnetic field with respect to time is equal to the first term (convection term). With that, the magnetic flux is frozen and the plasma arrangement of the magnetic field are fixed. The convection term represents the movement that explains the travelling magnetic field as a blob that may interfere the earth's electromagnetic wave in the earth atmosphere. Consequently, the term shows the behavior of solar radio burst in MHD where CME always disrupted the solar atmosphere (Gou et al., 2019). Abandoning the diffusive processes, it will restrict the behavior of changing plasma topology and no particle are free to mix along the field-lines in perpendicular order to the field (Fitzpatrick, 2014).

2.2.2 Other Related Type II Occurrence

On a bigger picture, the HWDA range of 55 to 65 MHz is study able for on-site ground-based centered detection of solar radio burst type II. Detecting CME is made possible through studying the space weather, one of which is closely related to solar radio burst type II. CALLISTO is one of current technologies that is up to in investigating solar radio burst type II, but there is no other instrument that totally focus on the scale of gaps between its fundamental and harmonic emissions. It is hard to identify short-lived solar radio burst type II, if it happens at the spatial resolution during the same time and frequency (Zucca et al., 2012). Such correlations for the solar radio burst type II occurrence is a valuable findings since it has a longer period of occurrence when compared to solar radio bursts type III. First identified complex solar radio burst type III data by ISEE-3 name it as "shock accelerated events" as it is related to solar radio burst type II (Gopalswamy, 2011). Looking through solar radio burst, a more frequent solar radio burst type III can be studied. An investigation of solar radio burst type III plays an important in forecasting solar energetic particle (SEP) event. Statistics have shown within 2 hour period, 59% of solar radio burst type III associates with type II presented 92% of SEPs occurs when both type II and type III are being detected in a period of time (Winter & Ledbetter, 2015). These exhibits an explanation the behaviour of solar radio burst type II often tailing solar radio burst type III (Thompson, 1959). But for a SEP event itself, it doesn't necessarily need to be associated with solar radio burst type III, if it is not accompanied by solar radio burst type II (Gopalswamy, 2011).

The association of type II and type III involved in forecasting SEPs (Winter & Ledbetter, 2015), but at low frequency, the observation which associates them may lead to articulate with hazardous CME. The CME may be catastrophic event and it may leads to the interplanetary shocks but most flares are motivated from coronal shocks (Zucca et al., 2012). Fort Davis have shown numbers of records solar radio burst type II is accompanied by groups of solar radio burst type III (Thompson, 1959). The plasma propagation of each type II and type III determines whether it has a slow drift or a fast drift differentiates the two solar radio bursts. Their relation signifies that studying solar radio burst type III is equally important as to studying solar radio burst type II.

2.3 Solar Storm Risk

Solar storm may be originated from solar flare and CME (Klein et al., 2018). Among expected threats, momentary blackouts, rerouting of aircraft, loss of a couple of satellites and "aurora borealis" are caused from solar storm. C-class flares have discernible impacts on Earth, M-class flares can cause brief radio power outages in the Polar Regions and X-class flares are recognized as significant occasions (Falco et al., 2019). This significant occasion can trigger overall radio power outages and radiation storms in the upper Earth atmosphere. The Earth's magnetic field changes after the collision of charged particles and magnetic fields for until a few hours or days.

Historically, the largest solar flare was recorded September 1, 1859 known as the Carrington flare (Marusek, 2007). In the modern world, such event would cause a noteworthy worldwide disaster. At the point when a CME strikes Earth, the compacted attractive fields and plasma in their leading edge impact the geomagnetic field like a battering ram. In a solar storm, the Earth's magnetosphere modifies when the CME plasma cloud strikes into the planet. These occurence are alluded to as a geomagnetic storm and may strike for few days. They opt to cause voltage varieties and actuate Geomagnetic Induced Currents (GICs). These GICs will flow through transformers, power gridlines and grounding points. A few amperes of GICs will cause transformers be crashed into half-cycle saturation where the core is magnetically soak on alternate half-cycle. Approximately as high as 184 amps GICs have been estimated in the United States in the neutral leg of transformers (Marusek, 2007). A solar storm can assault the gridlines over numerous points creating multi-point failure. Strong radio waves rom solar radio burst might interfere with global navigation satellite systems (Sato et al., 2019). Custom designed transformer may take a long time to repair. Economically, the damage may have a great impact even the power is restored within few hours. A noteworthy power outage in the Northeast U.S. is assessed to effectively surpass a few billion dollars in loss (Marusek, 2007). Power is fundamental to our industry, interchanges, transportation, trade, water supply and general social welfare.

2.4 Non-Thermal Processes

For this research, there are no temperature monitoring parameter and it is hard to identify thermal or non-thermal process. In 2009, Benz investigated the non-thermal process excluding the temperature parameter. By differentiating a non-thermal processes and emission of plasma origins, Benz stated, Solar Radio Burst Type III observation which originates at the corona, requires a high brightness temperature which explain the sun radio waves emission (Benz, 2009). Normally, non-thermal electron loses their kinetic energy in the coulomb field of the surrounding particle when it collides with plasma. Not only it stops a fast electron, but the targeted plasma is heated (Aschwanden, 2006). Radio emission mechanism can be divided into thermal and non-thermal processes. The generation of radio waves from the Sun can be best explain by the mechanisms. The process can be distinguish through the involvement of temperature parameter. A black body radiation is an example of thermal process as it involves temperature. While, a non-thermal process is simply a process that doesn't implies the temperature parameter.

2.4.1 Solar Radio Burst Type III

Solar Radio Burst Type III is a relativistic electron beam travelling along open magnetic field lines (Gopalswamy, 2011). Their fast frequency drift gain solar radio burst type III's known as fast drift burst. The duration is quite short up to seconds or minutes which usually appears in groups. It is also caused by high flare accelerated electron beams (Monstein, 2011).

There is still a strong debate going on the origin of electron of Solar Radio Burst Type III and still remain unresolved. An argument said the electron were accelerated at the flare reconnection site where shock arises from CME. New components appeared in august 2005, relating type III and type IV suggesting it stills occurs at flare site. The acceleration process of electron were thought to be accelerated at the flare site, but the other said it was shock accelerated. At long wavelengths, Solar Radio Burst Type III is ought to be not to be associated with major flares if it is without CME (Gopalswamy, 2011). A disastrous event like CME can be fatal, but most coronal shocks originates from flares (Zucca et al., 2012). This sum to relation of Solar Radio Burst Type III to solar flares is an important quest to be studied.

CHAPTER 3: METHODOLOGY

3.1 Setting Up Half Wave Dipole Antenna

A replica of Yunnan Astronomical Observatory (YNAO) in China technology, Half Wave Dipole Antenna (HWDA) Array is set up in University of Malaya's (UM) ground by means of research collaboration. The main intention is to have a VLBI array between the antennas in YNAO and UM where current tests are being done in UM observatory site. The events of solar atmosphere is make relevant with solar radio observation as it produce electromagnetic and particles radiation that impacts the Earth (White, 2007).

Solar Radio Burst type II can be hazardous in terms of it relation with the propagation of CMEs (Gopalswamy, 2016). Even with the current instrument it is difficult to observe earthward CMEs with a coronagraph. Till present, there is no direct measurement of the earthward CMEs speed recorded using the classical coronagraph approach (Klein et al., 2018). Low frequencies solar radio bursts probably originate geomagnetic disturbance, where energies from at which the layer of solar atmosphere released in solar flares, accelerate energetic particle and launch CMEs, clearly because most emission is a plasma emission (White, 2007). Statically, Fort Davis records Solar radio burst type II is accompanied by groups of solar radio burst type III (Thompson, 1959). Low frequency observation of the events of solar radio burst type III and type II investigation may lead to a groundbreaking inter connection with hazardous CME. Besides being easy to handle and relatively cheap, radio observation instrument is well protected from space hazards by Earth's atmosphere and magnetosphere (Klein et al., 2018).

3.1.1 Environmental Radio Survey

Before setting up the array, the radio frequency interference (RFI) of the observation site is studied to ensure the signals involved in this study. This survey is a crucial step to recognize the range of RFI. An observation is carried out for 24 hours to show an overview of the radio environment at the site. The setup of the survey is illustrated with the following block diagram as shown in the Figure 3.1.

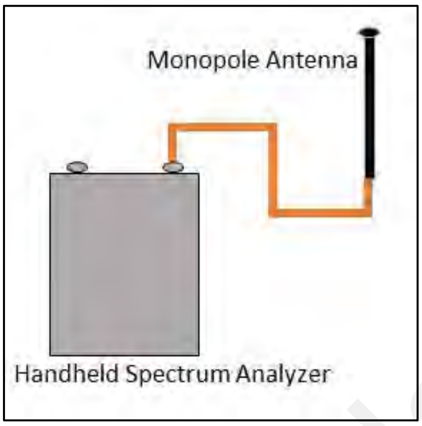

Figure 3.1: Block diagram of Radio Environment Survey Setup.

A handheld spectrum analyser is used in this survey to increase mobility at site. Once the monopole antenna is placed at the centre of the observation site it is connected to the handheld spectrum analyser using a coaxial cable. The 24-hour survey is done at 1859 on the 22nd of November 2016 till 1903 on the 23rd of November 2016 from 20 to 120 MHz at approximately 2 minutes interval to ensure the observation site is reliable for the research which at the range of 55 to 65 MHz. Each interval is saved into .csv file making 486 files in total. Figure 3.2 shows a print screen of one .csv file. The data are extracted using PYTHON with the program in Appendix A.

The 24-hour survey is shown on Figure 3.3 describing the radio environment of the site. The significant peaks of local broadcasting frequencies from 87 to 108 MHz doesn't relate to the research. By enlarging the survey, Figure 3.4 confirms that the range used in this research of 55 to 65 MHz is not affected. Inferring, the research using the HWDA array through the observation site will not be affected knowingly by RFI

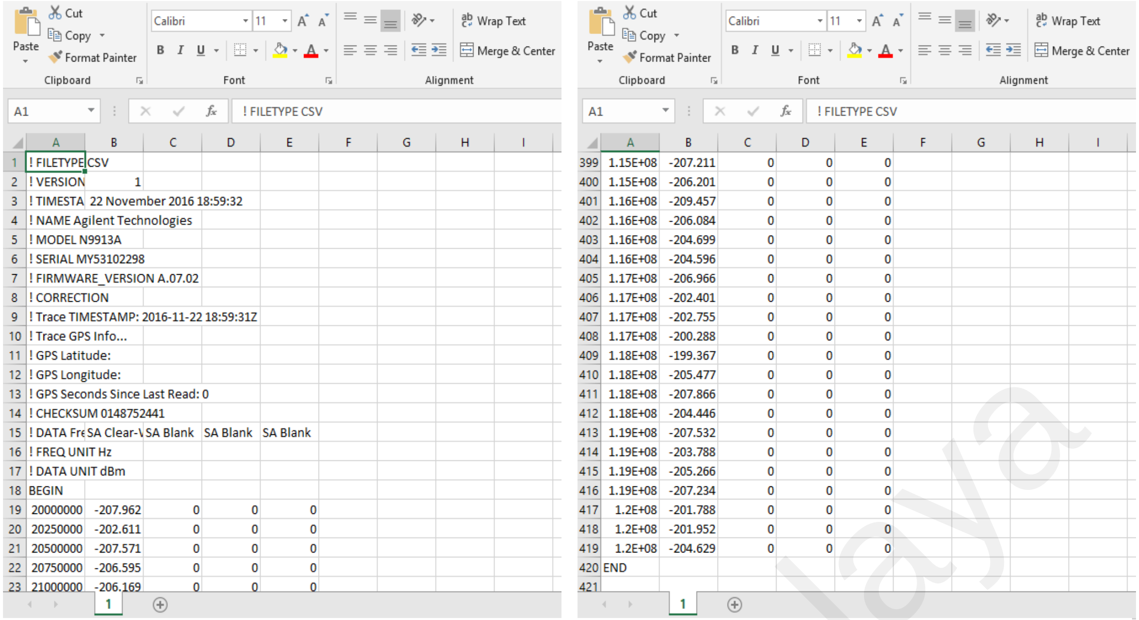

	A	B	C	D	E
1	! FILETYPE	CSV			
2	! VERSION	1			
3	! TIMESTA	22 November 2016 18:59:32			
4	! NAME Agilent Technologies				
5	! MODEL N9913A				
6	! SERIAL MY53102298				
7	! FIRMWARE_VERSION A.07.02				
8	! CORRECTION				
9	! Trace TIMESTAMP: 2016-11-22 18:59:31Z				
10	! Trace GPS Info...				
11	! GPS Latitude:				
12	! GPS Longitude:				
13	! GPS Seconds Since Last Read: 0				
14	! CHECKSUM 0148752441				
15	! DATA Fre	SA Clear-V	SA Blank	SA Blank	SA Blank
16	! FREQ UNIT Hz				
17	! DATA UNIT dBm				
18	BEGIN				
19	20000000	-207.962	0	0	0
20	20250000	-202.611	0	0	0
21	20500000	-207.571	0	0	0
22	20750000	-206.595	0	0	0
23	21000000	-206.169	0	0	0

	A	B	C	D	E
399	1.15E+08	-207.211	0	0	0
400	1.15E+08	-206.201	0	0	0
401	1.16E+08	-209.457	0	0	0
402	1.16E+08	-206.084	0	0	0
403	1.16E+08	-204.699	0	0	0
404	1.16E+08	-204.596	0	0	0
405	1.17E+08	-206.966	0	0	0
406	1.17E+08	-202.401	0	0	0
407	1.17E+08	-202.755	0	0	0
408	1.17E+08	-200.288	0	0	0
409	1.18E+08	-199.367	0	0	0
410	1.18E+08	-205.477	0	0	0
411	1.18E+08	-207.866	0	0	0
412	1.18E+08	-204.446	0	0	0
413	1.19E+08	-207.532	0	0	0
414	1.19E+08	-203.788	0	0	0
415	1.19E+08	-205.266	0	0	0
416	1.19E+08	-207.234	0	0	0
417	1.2E+08	-201.788	0	0	0
418	1.2E+08	-201.952	0	0	0
419	1.2E+08	-204.629	0	0	0
420	END				
421					

Figure 3.2: Print screen of one .csv file saved at 1859 on the 22nd of November 2016.

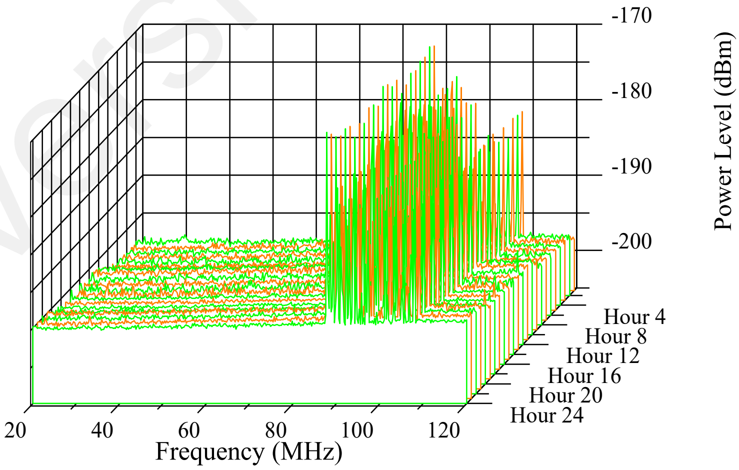

Figure 3.3: 24-hour average RFI at observation site between 20 to 120 MHz.

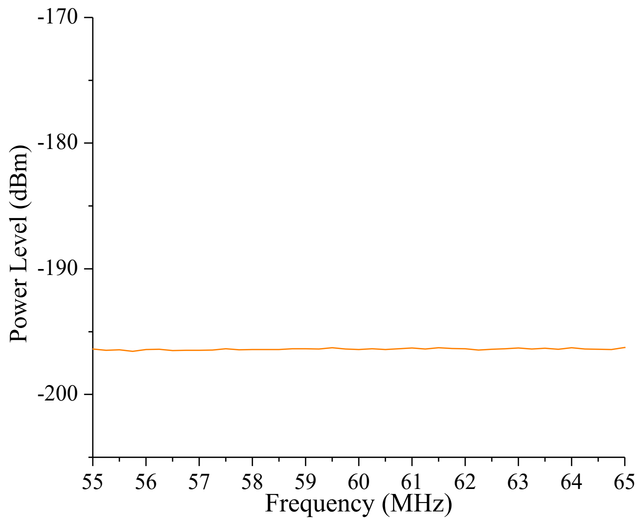

Figure 3.4: 24-hour average RFI at site for HWDA array frequency.

3.1.2 Half Wave Dipole Antenna Array

The array consists of four twin-dipole antennae which can be shown in Figure 3.5 (a). Each twin-dipole antenna is a dual oscillator, symmetrical broadband, and orthogonal as shown in Figure 3.5 (b). Each twin is paired in placed of inverted V as shown in Figure 3.5 (c). The pole of the antenna is 1m like indicated if Figure 3.5 (c), the pole itself existed to give height for the blade to stand, there is no conduction of electricity between the pole and blade, it is there as a cane. A half wave dipole is an antenna with two arm blades such that the blades are angle to the pole and making it an inverted V shape. The inverted V itself makes a simplified HWDA. But for this setup, one unit of HWDA came from two inverted Vs. Each inverted V is connected to a receiver where signals are being capture. A receiver receives signals from two blades, so two input signals are being capture by the receiver. A unit of HWDA is made of two inverted Vs, one receiver receive two input signal from one inverted V which contain two blades, so two receiver is required for one unit of HWDA. The two input signals then carries one output signal, where the output signal can be capture by another unit of capturing device in the control room. For one unit of HWDA, two receivers are attached to the pole. The pole again act as cane holding two receivers and a direct circuit is also connected from the control room to the receivers to attain its power supply. For short, one unit of HWDA contains a pole with the height of 1m, 4 blades with the length of 1.5m, two receivers and data capture instrument. Power is being supplied to the receivers and data capture instrument. One unit of HWDA is made of two inverted Vs, where the Sun radio information is being capture by two input signal from one inverted V via one receiver. The inverted V is made of two blades that produce one output signals and data is recorded by the data capture instrument. One blade with a length of 1.5m makes a hypotenuse to the pole height of 1m. An angle is present. This is to ensure the blade would capture the Sun radio signal, because a flat horizontal of the blade would reflect the sun signal to the environment and a vertical blade would not capture any signal. 3m distance between the antennae ensure that the antenna units are not touching each other. The 4m represent the distance between the array of HWDA to the control room. The setup of HWDA array is furthered away from the control room to ensure that all signals were not blocked by the building itself. This is to ensure that all present Sun radio signals are being captured and detected. After returning from World War II, low frequency of below 100 MHz were pioneer of radio research. The frequency can be used as a direct measure of density and indirect measure of emission height (White, 2007). The twin dipole antenna is made of two HWDA at frequency range of 30 to 70 MHz at 40 MHz bandwidth where each twin-dipole antenna is completed with two receivers for one complete HWDA system, filters the coverage from 55 to 65 MHz. in other words, one complete HWDA system consists of a twin dipole antenna. Orthogonally, the HWDA blades are facing North, East, West or South direction where each twin-dipole antenna is either placed East-west or North-south. This is to ensure that each complete HWDA system (twin dipole antenna) captures signals from all direction. Their other technical specifications include gain of 6 dBi and VSWR < 3:1.

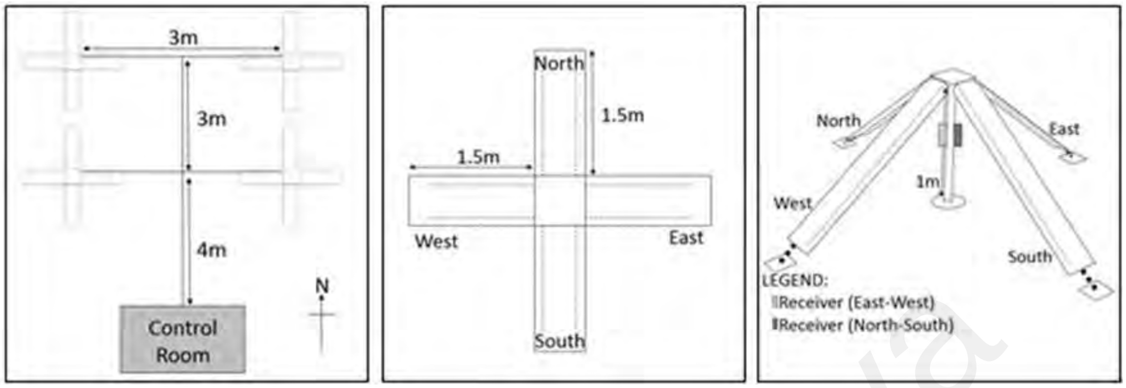

(a) Array view (b) Top view (c) 3D view

Figure 3.5: HWDA setup views.

Each twin dipole is connected to its own receiver become an input signal to the data acquisition circuit. From the data acquisition circuit, signals are readable to computer and all the signals are processed in the computer until a spectrogram is obtained. Each of the receiver operates at the voltage of 15V and the current of 0.32 A.

3.1.3 Receiver

Through the collaboration between UM and YNAO, the receiver has been provided. The provided receivers are tested for its band pass filtering. Figure 3.6 shows a block diagram how the setup of the test being held. To capture a signal, each receiver have two signal input ports correlate signals into one output signal. The receiver have two signal inputs (RF in) because one inverted V have two blade, the signal from one inverted V can be correlate using HX62A correlator. A receiver is connected to other instrument such a handheld spectrum analyser or the antenna using a BNC connector. A BNC connector is connect/disconnect radio frequency connector to the coaxial cable. The signal input (RF in) in Figure 3.6 is connected to handheld spectrum analyser because it is being tested. The functionality of the receiver have to be tested to ensure both RF in(s) can receive signals. Each port are being tested individually using the network analyser mode on the handheld spectrum analyser to ensure the solar radio signal are being captured effectively. A network analyser mode generates signal and analyse spectrum at the same time. While being tested, the tested input port received signal at 20 to 120 MHZ whereas the other port is being hindered using a 50 Ω terminator. The component is a terminator with a resistance of 50 Ω. Although the terminator has a resistance of 50 Ω, it is not a resistor, a terminator works to terminate one signal of the two inputs. The setup is to ensure the receiver is working efficiently. When one terminator is connected to one input, there is no open circuit, readings can be taken. Every ports, i.e. inputs and output, need to be in a close circuit, so that current can flow and readings can be made. The handheld spectrum analyser instrument acts as signal generator and a spectrum analyser. Figure 3.7 show that upon filtering the signal quickly pickups until it reach approximately 55 MHz and the signal is then suppressed back at 65 MHz. Figure 3.8 shows the captured signal is allowed at the range of 55 to 65 MHz but the bandpass is not smooth towards the end as there is a slight peak presence when the signal is being suppressed indicating some of the filtered unwanted frequency managed to escape the bandpass filters. In other words, Figure 3.7 shows a good bandpass filtering while Figure 3.8 shows a bad bandpass filtering indicating a faulty receiver. In this research, preferably a receiver performance works at its best with an ideal bandpass filtering, any suspicion on faulty receiver is send back to YNAO for repairing purposes.

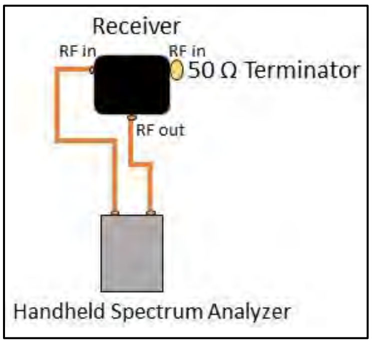

Figure 3.6: Block diagram of Bandpass testing Setup.

The receiver is based on integrated microwave module design. Figure 3.9 shows a schematic block diagram of the receiver. The receiver consists of band-pass filters, monolithic amplifiers and a correlator. Each of the input signals came from each of the antenna arm. When a terminator is added no signal would be correlate because one of the signal would be terminated.

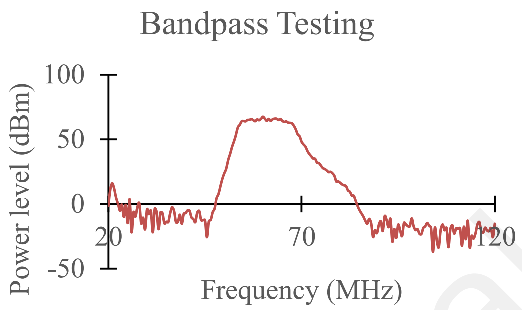

Figure 3.7: Good bandpass filter.

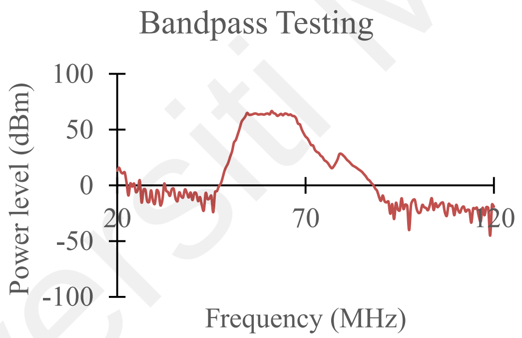

Figure 3.8: Bad bandpass filter.

A band-pass filter works by cancelling out the unwanted frequencies, and only allows for signals to work at a certain range (Kuphaldt, 2007). Two types of band-pass filters are used in the receiver's circuit, BPF-C45+ and BPF-A60+. The double filtering optimizes the sensitivity of the receiver. BPF-C45+ has a gain response with frequencies range from 30-70 MHz, while BPF-A60+ range from 55-65 MHz. Normally, BPF-C45+ is used in military communication and BPF-A60+ is used to test equipment. Both of the band pass filters are commonly used in receivers and transmitters. Both are great at harmonic rejection resulting the unwanted signals being suppressed. Monolithic amplifiers, GALI-74+ is used to ensure no involving signal are wasted after being filtered. Both input signal (RF in) for each of the receiver is deduced using a HX62A correlator. Overall, the receiver performs at band pass of 55 to 65MHz with a total gain of 52dB, noise temperature of 320K and the flatness of ± 1dB. As shown in Figure 3.4, the frequency between 55 to 65 MHz have no significance interference involved will disturbed the signal at the band of the receiver's performance. The receiver acts as to receive and capture signal, clearly a half wave dipole acts with two poles, in this research we refer as blades because it flat to cover the range of 55 to 65 MHz. the simplest way to ensure one inverted V is working which is the simplest unit of a HWDA antenna is to correlate both signals from the two blades. The receiver received signals from two signal inputs or RF in represents each blade is being correlated into one signal in a receiver. The half wave dipole is best define as an antenna with shortest resonant length of half wavelength long, so one blade only represents a quarter length. A receiver completes a HWDA design such that both quarter length is being correlated into a half wavelength, by taking note that a HWDA only works with half wavelength resonant length.

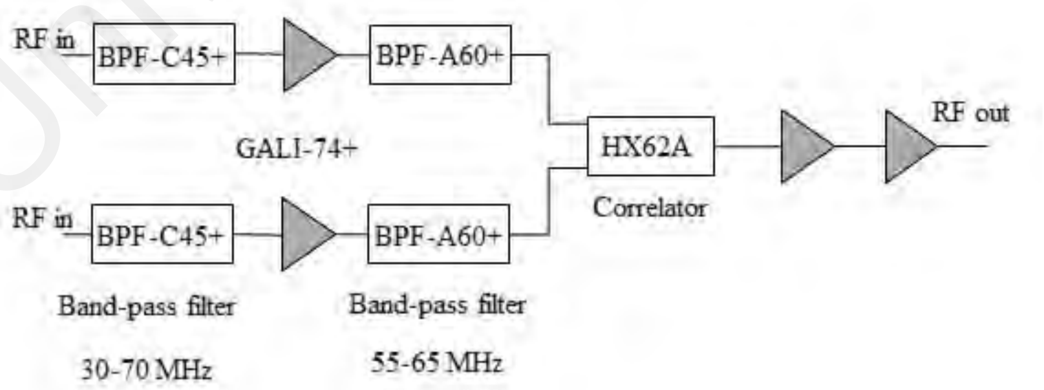

Figure 3.9: Schematic block diagram of a receiver.

3.2 Collected Sample

From the HWDA antenna, the spectrum of between 55 to 65 MHz is collected. The collected data is saved as .csv files in a folder. Each file represents a period of time, with its sets of frequency and power level. One compilation of all period is compute using the following python scripts in Appendix B before it is plotted into light curves.

Every real-life data is compared to the CALLISTO data to ensure it is a Solar Radio Burst type. Normally, for Solar Radio Burst research, the data is interpreted as spectrogram. Many of the spectrograms can be accessed through an online database such as the e-CALLISTO or other related solar radio burst sites. For the e-CALLISTO database, the spectrogram can be downloaded as a FITS image. These spectrograms may have Solar Radio Burst from the Sun or radio frequency interference from the surrounding. Their patterns can be distinguished clearly according to each type characteristics, shape and bandwidth. To ensure which type is being tested each collected or suspected burst spectrum from CALLISTO is tested individually. All in all, the half wave dipole antenna will compliment to the CALLISTO system, at the bandwidth of 55 to 65 MHz. Thus, for future preferences it will give a better view on the gap to a very narrow edges of the fundamental and the harmonic frequencies for solar radio burst type II.

3.2.1 CALLISTO spectrogram analysis

Compound Astronomical Low-Cost Low-frequency Instrument for Spectroscopy and Transportable Observatory (CALLISTO) is technology developed by Christian Monstein's research team of ETH Zurich to investigate the Solar Radio Burst phenomena. Their spectrum can be accessed online through e-CALLISTO database as a free source. In principal, the CALLISTO operates at the frequency of 45 MHz until 870 MHz. where every minute of spectrograms around the world is being saved into fits file into its database. The spectrograms with 15 minutes interval represent a 3D graph where the color contour between orange and blue shows the flux intensity of the radio emission. There are more than 144 CALLISTOs being installed all over the world to ensure its accessible solar radio burst occurrence for 24 hours daily such that there is a network to monitor the meter and decameter bands (Zucca et al., 2012). The HWDA provides a better focus with the range of 55 to 65 MHz resulting the spectrum will only appear as tiny specs within that range. Scheming into the five main types of solar radio burst the HWDA array data is compared to the e-CALLISTO data. Figure 3.10 shows an illustration of solar radio bursts' types.

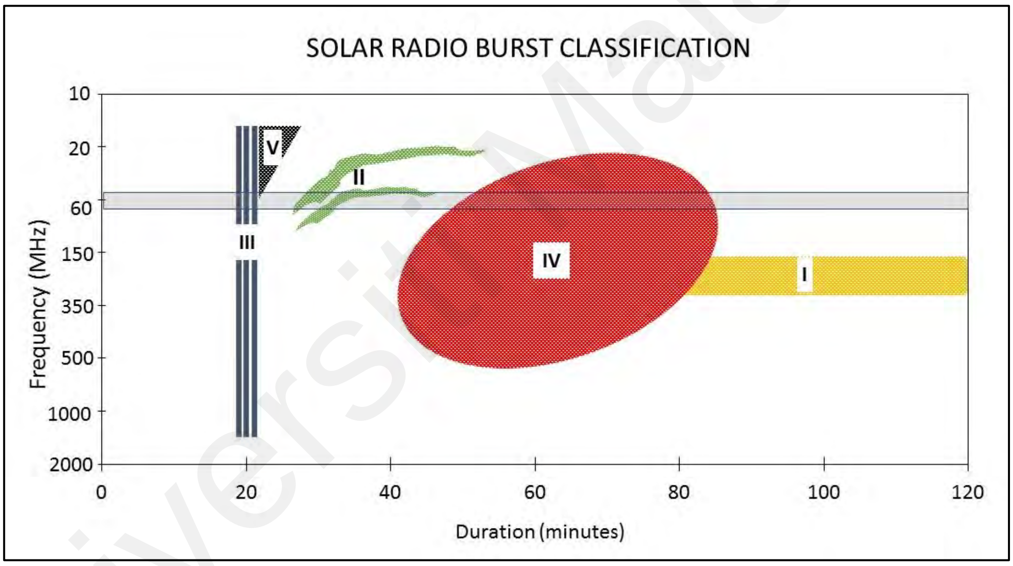

Figure 3.10: Five main types of solar radio burst with indicated HWDA frequency of 55 to 65 MHz.

By referring to Figure 3.10, at the range of 55 to 65 MHz only solar radio burst type III, type II and type IV can be detected with HWDA antenna. Any significance spectrum of the HWDA indicated these three types. A successful installation of HWDA is indicated if the detected spectrum (or peaks) in HWDA coincides with the three types in e-CALLISTO. Hence, e-CALLISTO spectrum will verify the detection of solar radio burst and its type by HWDA.

The involved solar radio burst is also being compared through linear fitting to correlate its involvement with solar flare. The light spectrum of solar flare can be obtained using National Oceanic and Atmospheric Administration (NOAA) database which available online for public accessed. NOAA is an American scientific agency that handles Geostationary Operational Environmental Satellite (GOES) that can provide solar flare data, where the data is represented by X-ray flux.

For future preferences, an overview study of solar radio burst type II using CALLISTO to indicate future used of the HWDA array. This will ensure the strong reasons of installing new technology (HWDA).

In this research, the installation of HWDA is successful with the detection of solar radio burst type III.

3.3 Other Related Theories and Calculation

Other physical parameters of the detected burst are then carefully studied from both spectrum from CALLISTO and HWDA using related theories mention in this section. With all physical parameters and solar flare comparison, the physical characteristics of the detected HWDA solar radio burst is known.

3.3.1 Plasma frequency

The observed frequency, f_o can be related to the plasma frequency, f_p using below relation, where $S = 2$ for harmonic frequency and $S = 1$ for fundamental frequency (Gao et al., 2014).

$$f_o = S f_p \tag{3.1}$$

Plasma frequency is the most fundamental time-scale in plasma physics.

$$\omega_p{}^2 = \frac{ne^2}{\varepsilon_0 m_e} \tag{3.2}$$

Taking note that plasma frequency is referred to electron plasma frequency, where ω_p is the angular frequency, n is the plasma density, ε_0 is the permittivity constant, e is the charge of electron and m_e is the mass of electron (Fitzpatrick, 2008). Since,

$$f_p = \frac{\omega_p}{2\pi} \tag{3.3}$$

where f_p is the plasma frequency. Therefore, by computing Equation (3.3) where e is 1.602×10^{-19} C, ε_0 is 8.85×10^{-12} Fm^{-1}, and m_e is 9.11×10^{-31} kg,

$$f_p = 9 \times 10^{-3}\sqrt{n} \qquad \text{(in MHz)} \tag{3.4}$$

3.3.2 Aschwanden & Benz density model

From the plasma frequency, the height of the radio burst emission can be deduced using the Aschwanden & Benz density model where it can be used to convert frequency of the radio emission into height of the radio emission, which is actually the height of the plasma particle of the solar radio burst.

Aschwanden & Benz (1995) density model,

$$n = \begin{cases} n_1\left(\frac{h}{h_1}\right)^{-p}, & h < h_1 \\ n_Q exp\left(\frac{-h}{L_n}\right), & h \geq h_1 \end{cases} \tag{3.5}$$

where n_1 is the transition density, n_{Q} is the electron density constraining barometric model base of the quiet corona, h is the height of radio emission, h_1 is the transition height, p is the polarity and L_n is the density scale height. This barometric density model is constrained by n_{Q} and L_n. For a smooth transition, the function is equal to the derivative of the function when it is continuous at $h = h_1$, this determine the value of h_1 and $n_1 = n$. From the model, we can say that,

$$h_1 = pL_n \quad , \qquad n = n_Q exp\left(\frac{-h}{L_n}\right) \tag{3.6}$$

Using the model, a few parameters are fixed, p = 2.38, L_n = 6.9 x 10^4 km and n_Q = 4.6 x10^8 cm^{-3} (Aschwanden & Benz, 1995). By manipulating the model, we managed to get Equation (3.7),

$$h = \frac{h_1}{\left(\frac{n_1}{n}\right)^{\frac{1}{p}}} \tag{3.7}$$

3.3.3 Gopalswamy model

In conjunction of categorizing the frequency range involved with HWDA array, the value of 60 MHz is used as an approximation. The value shows its significance in the gap between the harmonic and fundamental emissions of solar radio burst type II. The Gopalswamy model describes Solar radio Burst Type II which can be characterized by the power-law relationships, f (r) = $307.87r^{-3.78}$ – 0.14 (Kishore et al., 2016; Gopalswamy et al., 2013).

The Gopalswamy model (or power-law relationship) describes the relationship between the starting frequency, f, of a solar radio burst type II and the distance, r, associated with its CME leading edge. For a short-lived solar radio burst type II, it is hard to identify if the occurrences overlaps with other solar radio burst event it is hard to identify (Zucca et al., 2012), hence such findings would be greater than detecting solar radio burst type III. Their relation of preceding and tailing each other (Thompson, 1959) make researchers cross interlinked between the calculations ,where the integral intensity of solar radio burst type II were calculated using the same properties as such solar radio burst type III (Winter & Ledbetter, 2015). Gopalswamy model is used in estimating the physical parameters for solar radio burst type II. This is solely to approximate the gap between the emissions of solar radio burst type II. For other types of solar radio burst, the model can also be used by approximating the harmonic number, $S = 1$, where the observed frequency is equal to plasma frequency but this is the case where it is really necessary. The model should be the last alternative for other types since it is derived from solar radio burst type II (Gopalswamy et al., 2013). By manipulating Equation (3.4) with that model, an approximation of associated coronal magnetic field strength from the gap between the harmonic and fundamental emissions of solar radio burst type II is estimated. The shock speed, v, can be calculated by using Equation (3.4), Equation (3.8) and manipulating the drift rate, $\frac{df}{dt}$.

$$v = \frac{2L_n}{f}\left(\frac{df}{dt}\right) \tag{3.8}$$

Where the plasma frequency, f_p is used for fundamental emission, and the density scale height, L_n is shown in Equation (3.9) (Gopalswamy et al., 2009).

$$L_n = \left[\left(\frac{1}{n}\right)\left(\frac{dn}{dr}\right)\right]^{-1} \tag{3.9}$$

3.3.4 Density Enhancement Factor

The density enhancement factor is an indicator for solar activity level associated with higher density to active sun and lower density to quiet sun.

$$\frac{df}{dt} = -(8.7 \times 10^{-2})\ \frac{v}{c} \times f_{obs}\left[ln\left(\frac{0.54\,f}{S\sqrt{M}}\right)\right]^2 \tag{3.10}$$

Equation (3.10) shows a relation, where v is the estimated shock speed and c is the speed of light, df/dt is the drift rate, f_{obs} is the observed frequency, S is the harmonic number and M is density enhancement factor (Doddamani et al., 2014).

3.4 Observation Time

In the solar system, the Earth orbits the Sun at its on axis and it makes one complete rotation in 24 hours. The 24-hour rotation presents itself as day and night about half a day each at the equator. In calculating the best observation time, a few assumptions were made. The first assumption is the local sunrise is 0700 hrs, while the sunset time is 1900hrs. Figure 3.11 shows the polar angle, θ, and the azimuth angle, ϕ, of the radiation pattern.

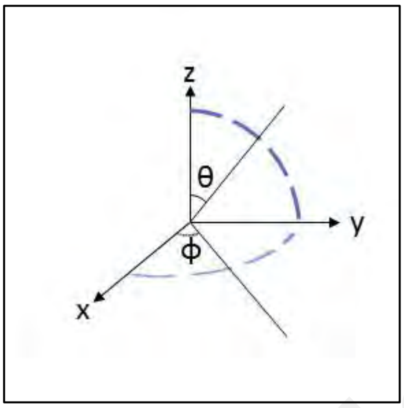

Figure 3.11: Three-dimensional plane indicating the polar and azimuth angles.

The field pattern, *E* is assumed as $E(\theta)=cos^2\theta$ in order to calculate the beam area, Ω, easily. Let's say the field pattern estimated the maximum radiation lobes. The beam area can be represented as in Equation (3.11) where $P_n\ (\theta, \phi)$ is the relative power (Kraus, Marhefka & Khan, 2006).

$$\Omega = \iint P_n\ (\theta, \phi)\ sin\ \theta\ d\theta\ d\phi \tag{3.11}$$

Figure 3.12 represents an overview of relating Figure 3.11 into estimating the observation time. Consider the y-plane is the horizon between the sky and ground. The observation is calculated using the polar angle, θ as an indicator for optimum observation time.

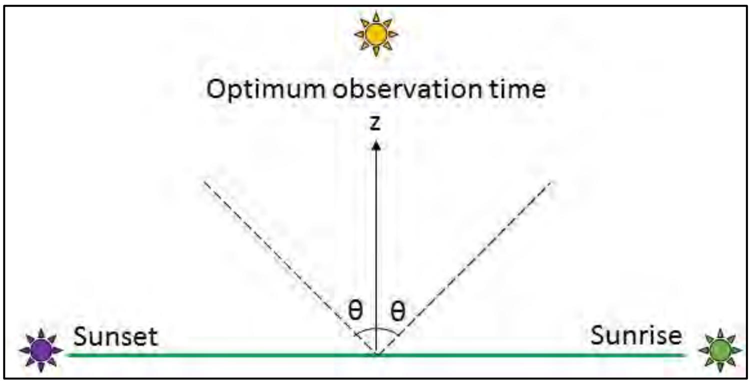

Figure 3.12: Representation of the sky and ground horizon in calculating the observation time.

Assume the azimuth angle, ϕ, covers the overall surface area from 0 to 2π. Based on a few basic mathematical manipulations, where the relative power is proportional to E^2 the beam area as shown in Equation (3.12) and gain, G, in Equation (3.13) were derived (Kraus et al., 2006; Orfanidis, 2002).

$$\Omega = \iint cos^4 \theta \, sin \, \theta \, d\theta \, d\phi \tag{3.12}$$

$$G = \frac{4\Pi}{\Omega} \tag{3.13}$$

G was calculated as 6 dBi, it estimated the polar angle to be 22.8˚. By deriving one horizon from sunrise to sunset as 180˚, the main optimum time was approximated at 1130 to 1430 local time. By preserving the optimum observation an extra 2 hours were taken into account. This will also indirectly be involving the probable minor side lobes. The observation time should be done between 0930 and 1630 hours daily.

CHAPTER 4: RESULTS

In this chapter, the results are discussed according to the objectives. Objective 1, to show the ability of detecting solar radio burst using the half wave dipole antenna are shown in Section 4.1 the preliminary results are discussed thoroughly. Objective 2, to identify the capability of HWDA by studying the relationship between solar radio burst type and solar flare are discussed specifically with events occurring dated 17th April 2017 in Section 4.2. Objective 3, to discover the potential of HWDA in investigating solar radio burst type through its distinct emissions, shock speed and drift rate in the last section.

4.1 Preliminary Results

One of institution that provide 24 hour solar monitoring is the US Air Force. Simple patrol instruments conducted radio observation using a typical parabolic antenna to observe the whole Sun flux density. Although there is no technical obstacle, there is no real time data providing the interplanetary travel times of CMEs (Klein et al., 2018). The half wave dipole antenna is providing data of solar radio burst. The proposition of CME propagation and solar radio burst type II is suggesting its relation in forecasting CMEs. Knowingly, the difference between a slow drift burst and fast drift burst might be due to their plasma propagation. This bid might be due to the accounts of solar radio burst type II often follows solar radio burst type III (Thompson, 1959). This thesis describes a novel research with a proven success by detecting solar radio burst type III.

A radio signal was present in the HWDA signal processing software on the 17th April 2017. The signals are converted into datasets in .csv files. A total of 942 files were saved. The files are manipulated into one large .csv files where it compiles all the time and power levels of each dataset using PYTHON. The programme is shown in Appendix C.

In Figure 4.1, the orange colored line indicates raw signal subtracted from averaged signals. The green colored line shows the fitting pattern of the overall signal. There is one significant pattern with peaks at approximately 10:47:04 a.m. (for 63.6 MHz frequency), 10:47:14 a.m. (63.4 MHz) and 10:47:25 a.m. (63.8 MHz). According to Figure 3.10, the range of HWDA 55 to 65 MHz falls in the range of solar radio burst, which is also the range of CALLISTO. The signals collected from HWDA on 17th April 2017 at 63.4 MHz, 63.6 MHz and 63.8 MHz falls at radio frequency range which is also in the range of CALLISTO. Since CALLISTO gives a bigger picture to HWDA, while HWDA focus at the range to gain better focus, so CALLISTO spectrogram gives out the solar radio burst type. By using the peaks on 17th April 2017 at 10:47:04 a.m. (for 63.6 MHz frequency), 10:47:14 a.m. (63.4 MHz) and 10:47:25 a.m. (63.8 MHz) from HWDA, the CALLISTO database is being investigated thoroughly during that given time and frequency.

Some solar radio burst event do associated with CME, but in this research the captured data coincides with solar flare not CME. A CME is a big hazardous event, but unfortunately it doesn’t occur during the research time frame. We investigated the CALLISTO spectrograms on the exact day and time in order to confirm the detection of a flare-related Solar Radio Bursts. This Solar Radio Burst event is indeed coincided with the flare detection made by GOES x-ray flux on the same day. The time interval between flare and burst is calculated to be less than 4 seconds. The burst detection verification of Solar Radio Burst type is detected by CALLISTO as in Figure 4.3. The CALLISTO data shows that the HWDA data is detecting solar radio burst type III on 17th April 2017 at the peaks. It was calculated that the time interval between the HWDA and CALLISTO detections was less than 3 minutes. By exploiting this phenomenon, it suggests that the small-scale properties of radio wave can detect solar radio burst. One possible solution may be pointed at different types of bursts detected by the two spectrometers. HWDA array has shown its capability of detecting signals of solar radio bursts.

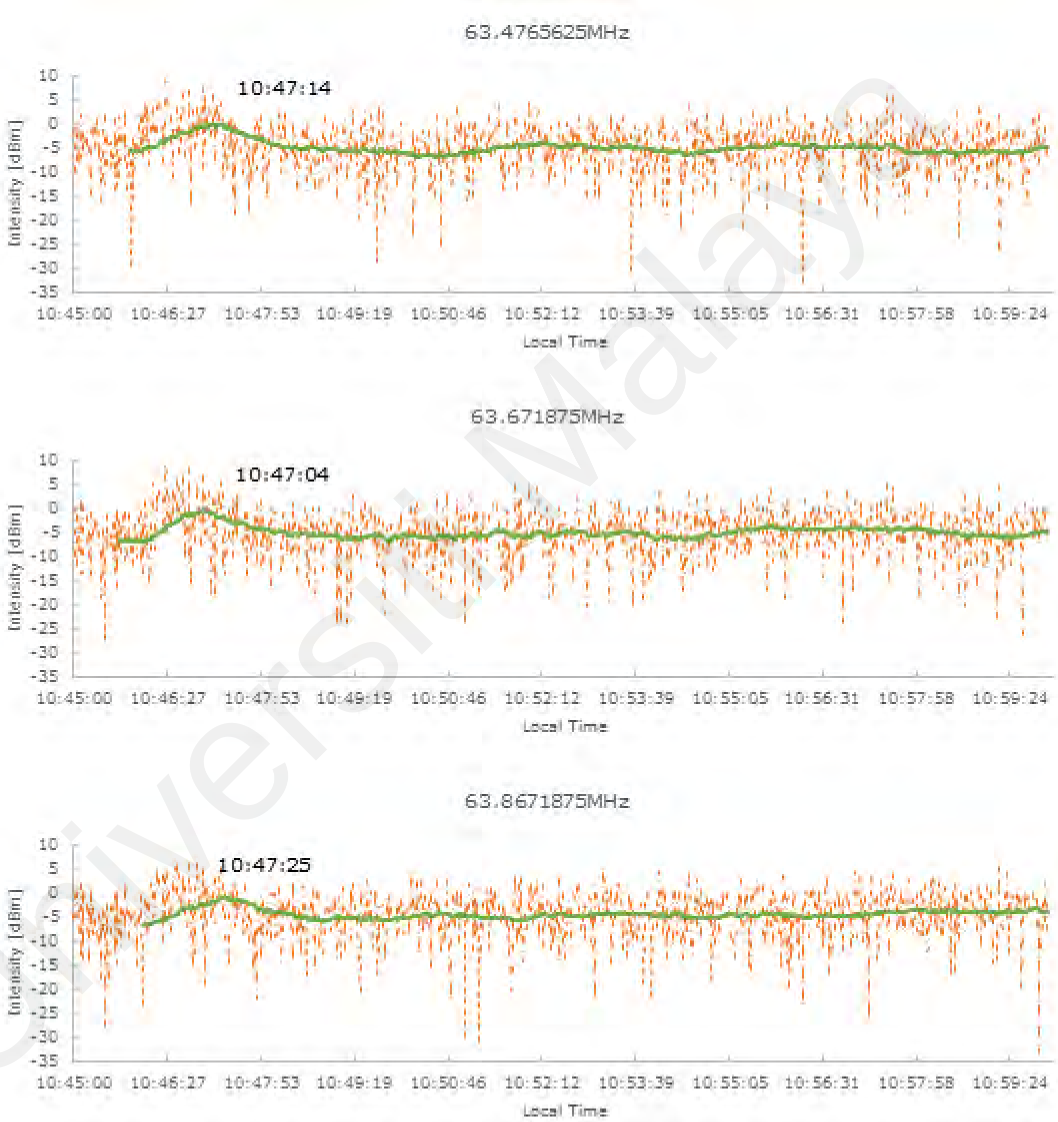

Figure 4.1: HWDA detection signal on 17th April 2017 at three separate frequencies (from top to bottom).

The green trendline in Figure 4.1 clearly shows the capability of HWDA to detect Solar Radio Bursts type III as it coincides with an observation from CALLISTO shown in Figure 4.3. In general, Solar Radio Burst type III is also known as fast drifting burst.

This type of radio emission is caused by flare accelerated electron beams propagating through the corona at high velocity (Monstein, 2011). The peaks in HWDA is capture in increasing intensity, instead of color contours like the regular spectrogram because this is just a preliminary results, to shows there is a detection. Looking at Figure 4.1, even a simple inversion into decreasing intensity axis shows an anomalies at then peaks into troughs still indicated there is a detection of solar radio burst. Furthermore, the peaks in Figure 4.1 indicated the intensity change in detection. The green lines in Figure 4.2 indicated from the green lines in Figure 4.1, the only datasets involve in Figure 4.2 is the frequency and local time located at the peaks of Figure 4.1. The green lines in Figure 4.2 have with the values 63.456625 MHz, 63.671875 MHz and 63.8671875 MHz showing that the frequency throughout the line is constant and it is not a variable inside the graph, only as an indication from Figure 4.1.

Figure 4.2 is a compilation of the green line trendline from Figure 4.1 showing the preliminary results of solar radio burst type III on 17th April 2017 from the HWDA at the frequency of 63.4 MHz, 63.6 MHz and 63.8 MHz. The red line is the fitting for the observed frequency where it also indicates the HWDA detecting two drift rates, 0.01 $MHzs^{-1}$ and -0.02 $MHzs^{-1}$. The results showed alternating signs of the drift rates signifying the capability of small range, 55 to 65 MHz of HWDA detection.

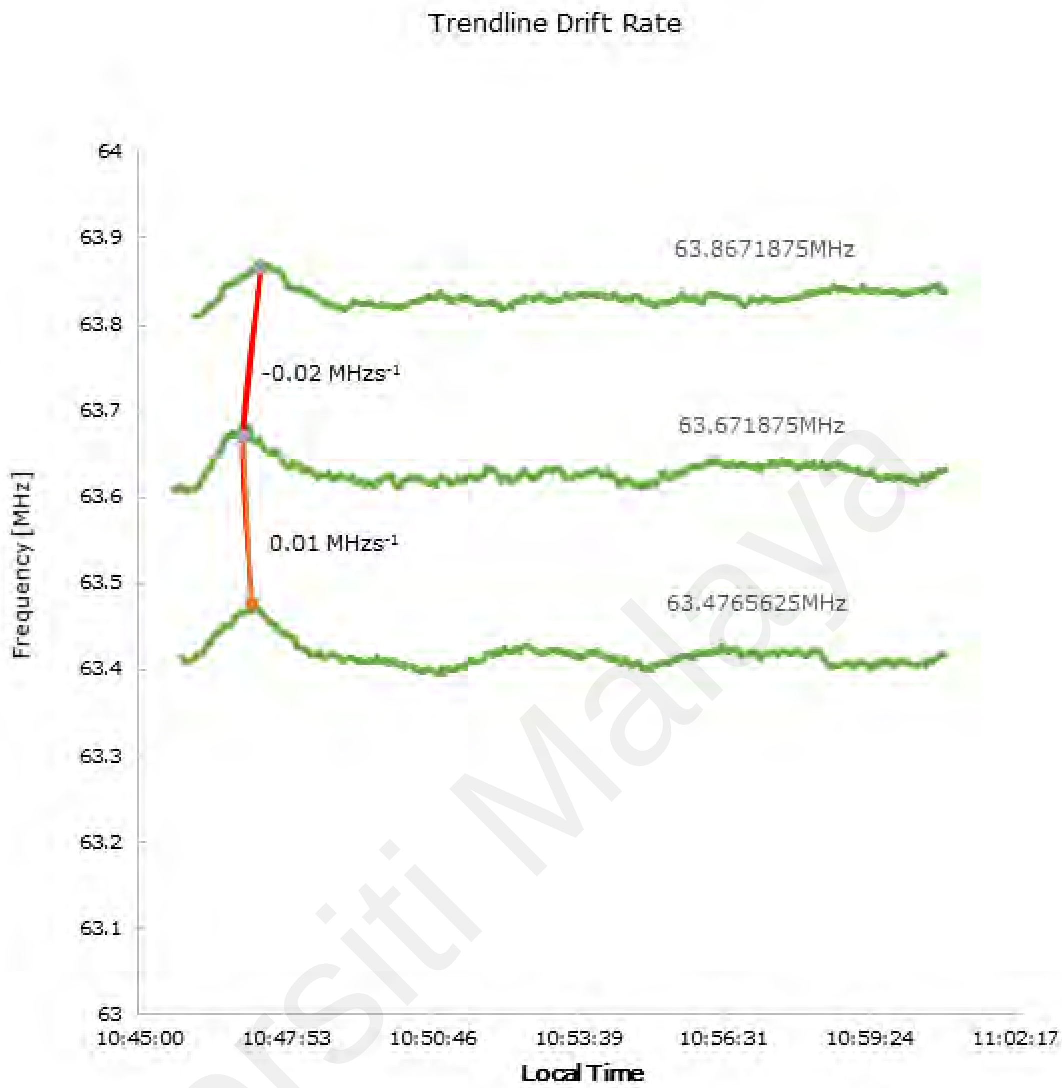

Figure 4.2: HWDA detection on 17th April 2017 with indicated drift rates.

Figure 4.3 show spectrograms obtained from the CALLISTO network at Almaty (in Kazakhstan) and Indonesia. They show Solar Radio Burst type III dated 17th April 2017 at approximately 02:50:37 UT to 02:51:00 UT. With the local time being +8 UTC, there is a solar radio burst type III at 10:50:37 a.m. to 10:51:00 a.m. Both spectrograms confirm type III between 54 to 89 MHz which coincides with the range of 55 to 65 MHz. The timing of the bursts occurrences coincides with the flare detection shown in Figure 4.5.

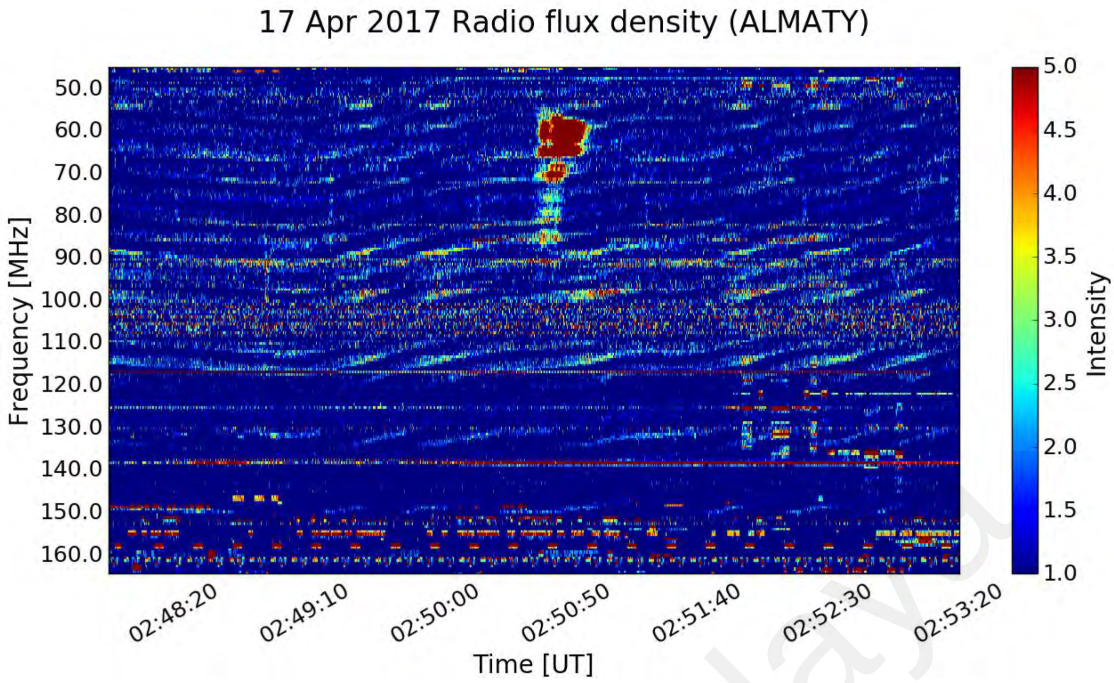

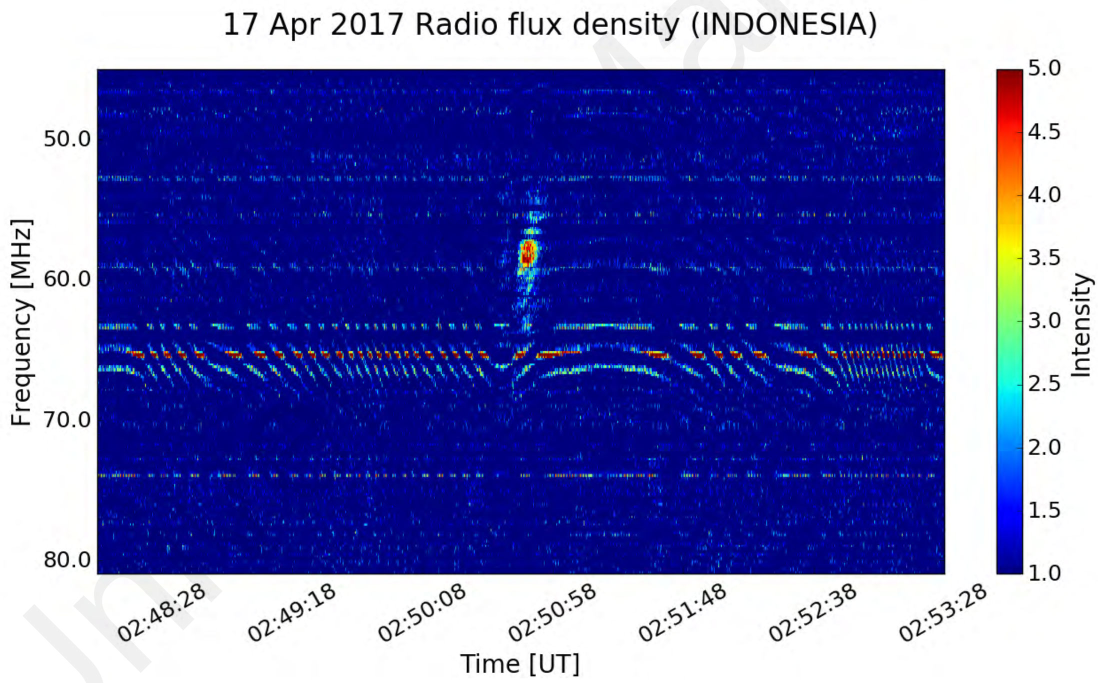

Figure 4.3: Solar Radio Burst Type III on 17th of April 2017 at approximately 02:50:37 UT to 02:51:00 UT for (top) Kazakhstan & (bottom) Indonesia.

The spectrogram shows the frequency axis (y-axis) in reverse order. This form indicates the highest frequency have lower height of radio emission from the solar surface compared to lower frequency. In other words, the descending order for frequency indicates the ascending distance of radio emission from the solar surface. The pattern difference between Kazakhstan and Indonesia site indicated a transient radio transmission. These may occur as there is a momentary variation in its physical parameters, i.e. current, voltage or frequency shifts.

Figure 4.4 show the spectrogram at Almaty (in Kazakhstan) dated 17th April 2017 at approximately after 02:49 UT. With linear approach, the Solar Radio Burst type III shows drift rates of -2.59 MHzs^{-1}, -4.55 MHzs^{-1}, and -1.91 MHzs^{-1}.

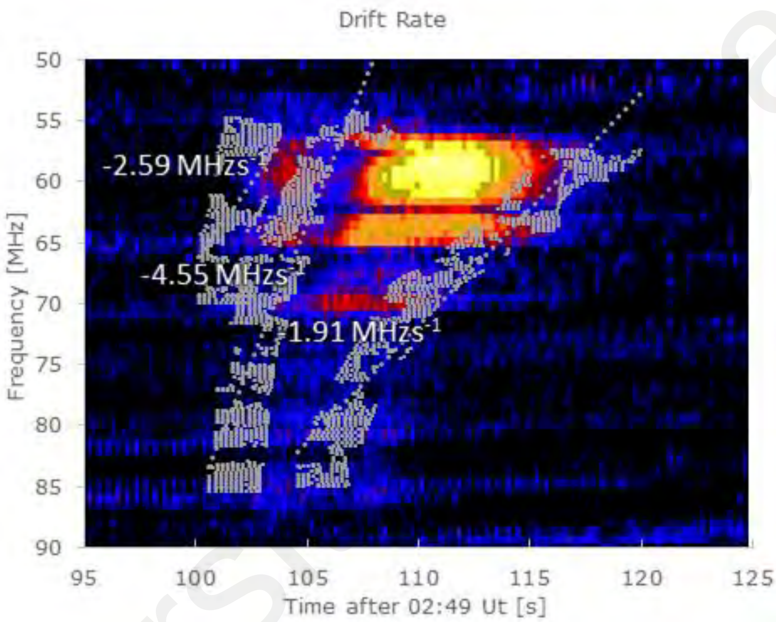

Figure 4.4: Solar Radio Burst Type III on 17th of April 2017 at approximately after 02:49 UT for Kazakhstan with 3 indicated drift rate linear approach.

4.2 Solar Radio Burst and Solar Flare Relation

An instrument is just a tool if there is no significant object to be studied. Proven science behind HWDA can be recognized through CALLISTO and GOES. The capability of HWDA are distinct through the relationship between solar radio burst type III by CALLISTO and solar flare by GOES. Figure 4.5 shows a CALLISTO spectrum at Almaty, Kazakhstan of a solar radio burst type III at 59.75 MHz on 17th April 2017 and its respective GOES X-ray Flux. The time series were chosen because it has the highest intensity for the radio spectral spectrogram. The GOES X-ray Flux, begin at

0217 UT, maxes at 0247 UT and ends at 0310 UT is classified class C 2.0 solar flare. Both events show a ratio R^2 value of GOES x-ray Flux to the time series of 0.94. For time series graph, the R^2 value represents the variation of solar radio burst intensity depends on time, while the R^2 value in GOES x-ray flux represents the variation of solar flare intensity depends on time. This indicates a strong correlation relationship between the solar radio burst and solar flare of that particular date. Another aim of the HWDA is to find such correlation for the case of solar radio burst type II (since it has a longer period of occurrence when compared to Solar Radio Bursts type III).

A time series graph represents the solar radio burst data where the R^2 value shows the variation of radio intensity over time, while the GOES x-ray Flux represents the solar flare data where the R^2 value shows the variation of x-ray flux intensity over time. The ratio of GOES x-ray Flux to the time series clearly shows the ratio of solar flare data to solar radio burst data, indicating the correlation of the time series occurs within the time frame of solar flare. This is clearly supported by Tandberg-Hanssen (1957), by stating a correlation between solar radio burst and solar flare because the burst occurs within the range of solar flare.

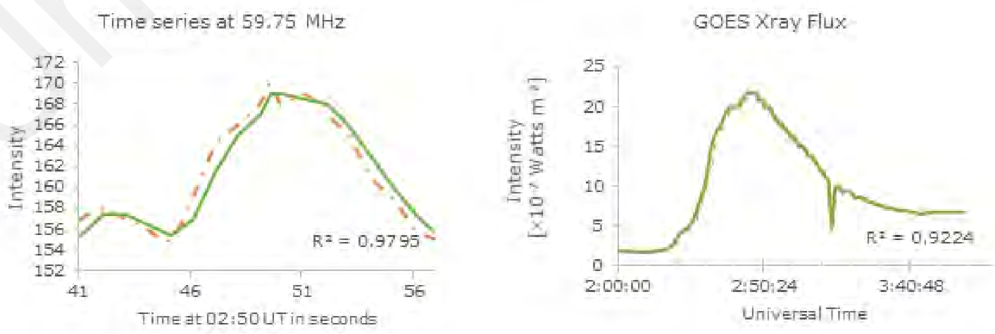

Figure 4.5: Selected CALLISTO spectrum at 59.75 MHz & GOES X-ray Flux on 17th April 2017 showing the ratio of R^2 value from GOES X-ray Flux to the time series at approximately 0.94. The green line represents signals at time series and GOES x-ray flux, respectively.

Coincidently, a number of events occur on 17th April 2017. The events are used to study the relationship between solar radio burst type III and solar flare. For each spectrogram, a 2D line spectrum is plotted by choosing the highest intensity for the radio spectral spectrogram. Figure 4.6 shows a CALLISTO spectrum at Almaty, Kazakhstan of a solar radio burst type III, its time series at 115.438 MHz on 17th April 2017 and its respective GOES X-ray Flux. The GOES X-ray Flux, begin at 0554 UT, maxes at 0558 UT and ends at 0602 UT is classified class B 4.0 solar flare. Figure 4.7 shows a CALLISTO spectrum at Blein, Switzerland of a solar radio burst type III, its time series at 36.438 MHz on 17th April 2017 and its respective GOES X-ray Flux. The GOES X-ray Flux, begin at 0713 UT, maxes at 0721 UT and ends at 0727 UT is classified class B 7.1 solar flare. Figure 4.8 shows a CALLISTO spectrum at Glasgow, Scotland of a solar radio burst type III, its time series at 55.313 MHz on 17th April 2017 and its respective GOES X-ray Flux. The GOES X-ray Flux, begin at 1440 UT, maxes at 1446 UT and ends at 1450 UT is classified class B 3.6 solar flare. Figure 4.9 shows a CALLISTO spectrum at Roswell, Georgia, United States of a solar radio burst type III, its time series at 29.811 MHz on 17th April 2017 and its respective GOES X-ray Flux. The GOES X-ray Flux, begin at 2121 UT, maxes at 2142 UT and ends at 2153 UT is classified class B 7.5 solar flare.

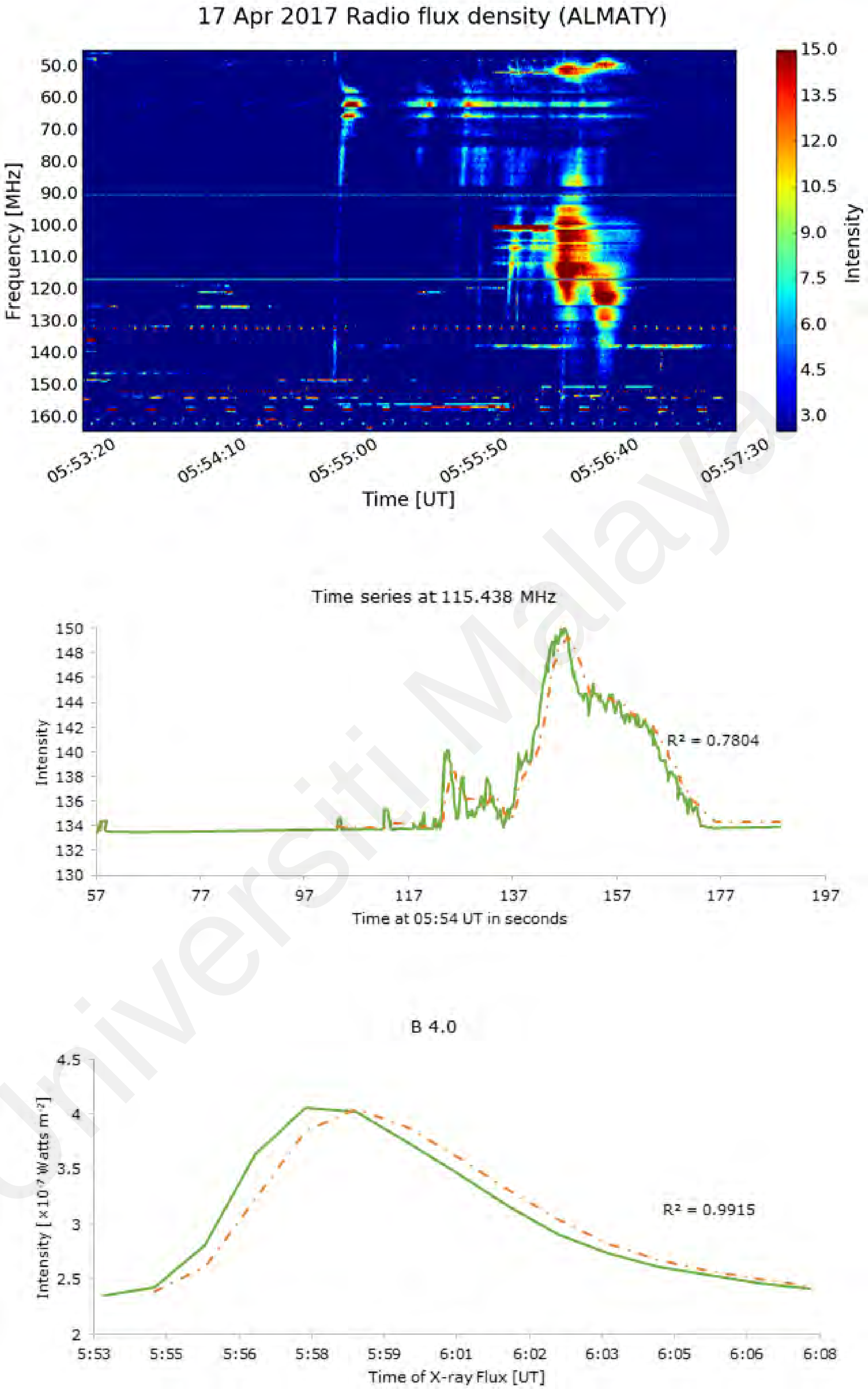

Figure 4.6: Selected CALLISTO spectrum at Almaty, Kazakhstan of a solar radio burst type III, its time series at 115.438 MHz on 17th April 2017 and its respective GOES X-ray Flux.

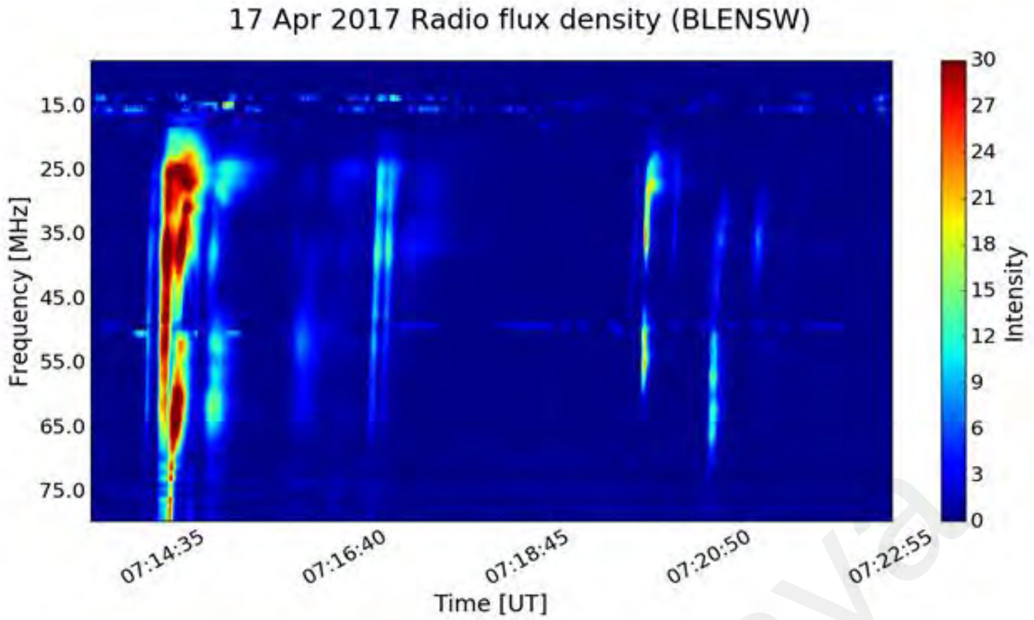

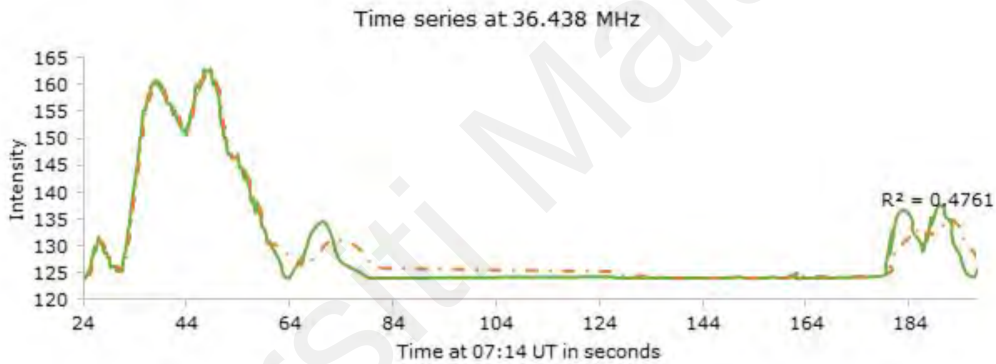

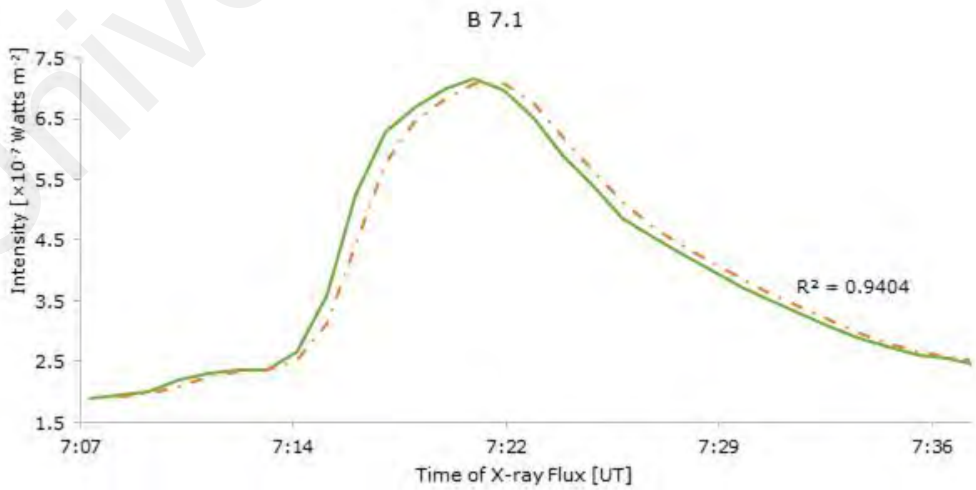

Figure 4.7: Selected CALLISTO spectrum at Blein, Switzerland of a solar radio burst type III, its time series at 36.438 MHz on 17th April 2017 and its respective GOES X-ray Flux.

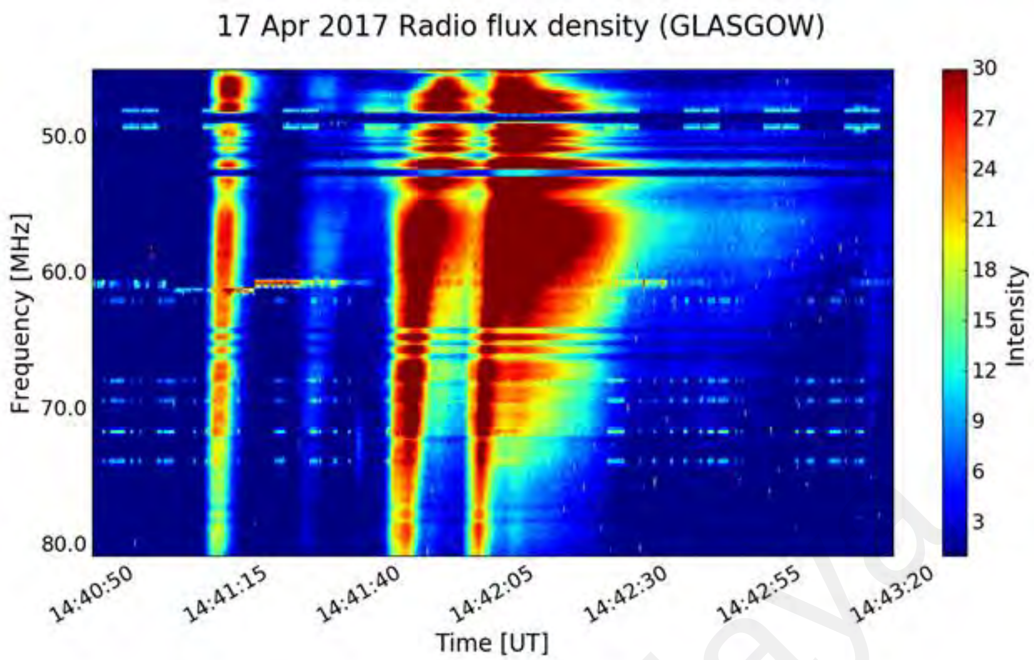

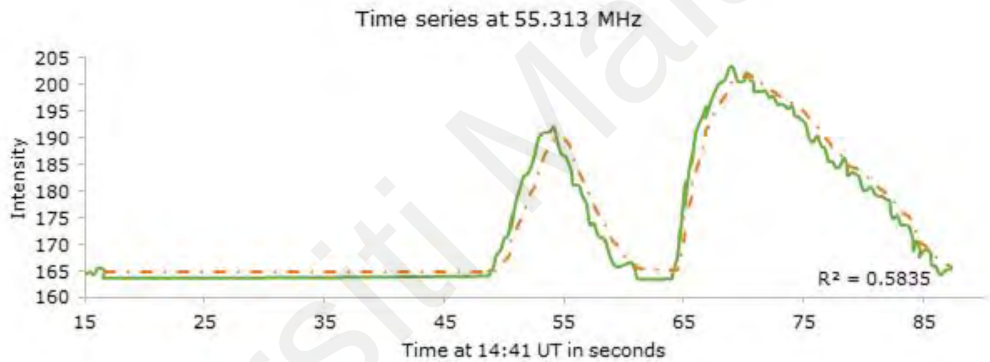

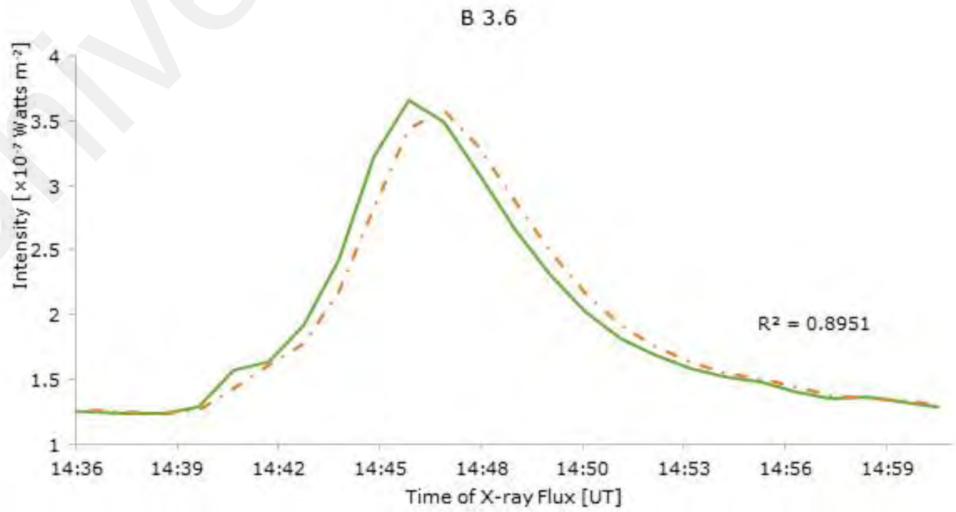

Figure 4.8: Selected a CALLISTO spectrum at Glasgow, Scotland of a solar radio burst type III, its time series at 55.313 MHz on 17th April 2017 and its respective GOES X-ray Flux.

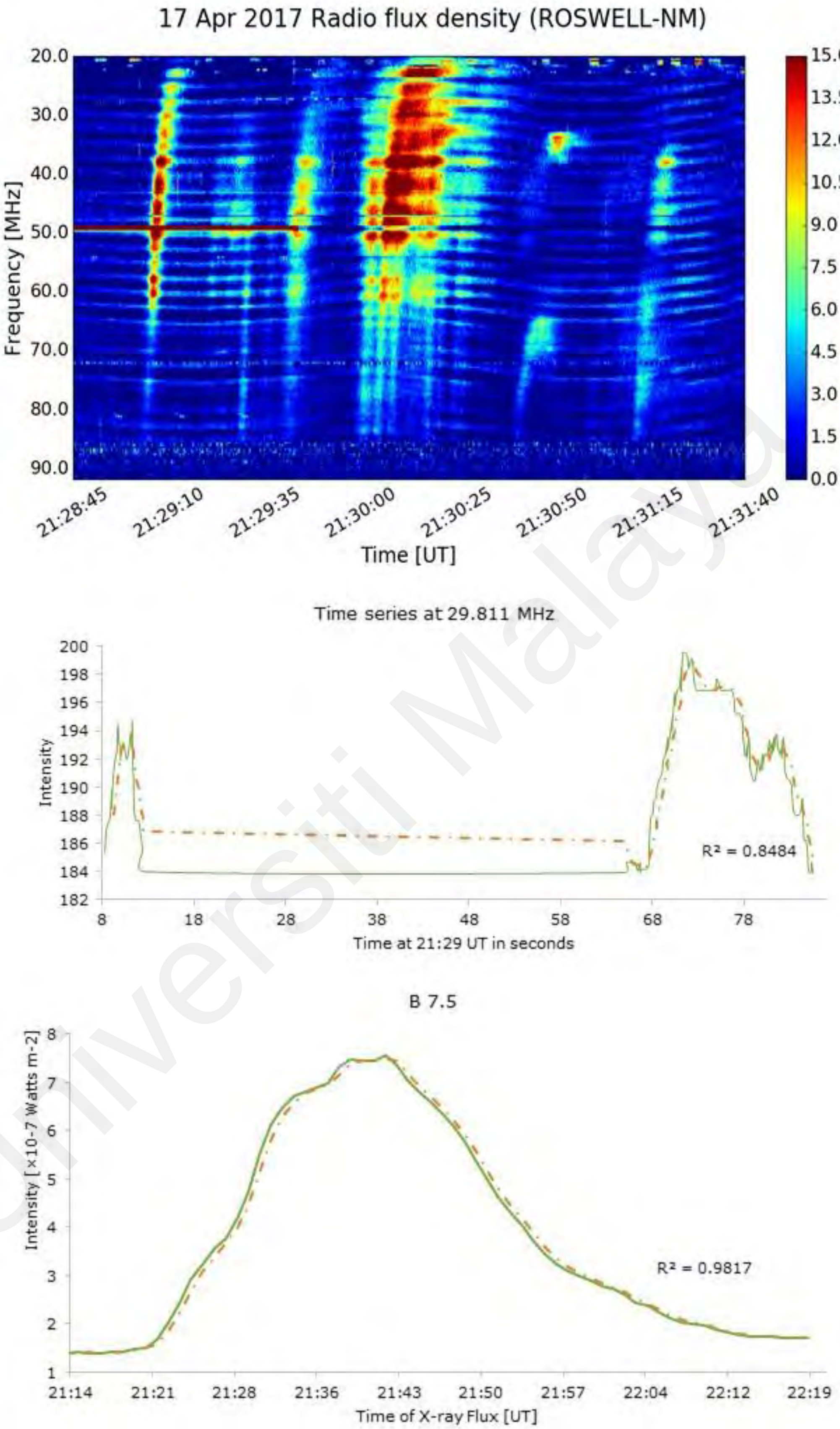

Figure 4.9: Selected CALLISTO spectrum at Roswell, Georgia, United States of a solar radio burst type III, its time series at 29.811 MHz on 17th April 2017 and its respective GOES X-ray Flux.

The green line represents signals at time series and GOES x-ray flux, respectively. While the orange dotted line shows the fitting of the curve with its respective R^2 value. Knowingly, the correlation increases with the importance of the flare, flare and burst are two exhibits the origins of a common disturbance, there is a positive correlation since the Sun burst smoothly within 10 minutes range of the solar flare occurrence (Tandberg-Hanssen, 1957). Figure 4.10, shows the timeline of GOES x-ray flux and R^2 value correlations. The timeline shows for all the events of solar flare on 17th April 2017. The indicated peaks show the solar flare that coincides with solar radio burst type III detected by CALLISTO. Where C 2.0 solar flare maxes at 0247 UT, B 4.0 solar flare maxes at 0558 UT, B 7.1 solar flare maxes at 0721 UT, B 3.6 solar flare maxes at 1446 UT and B 7.5 solar flare maxes at 2142 UT.

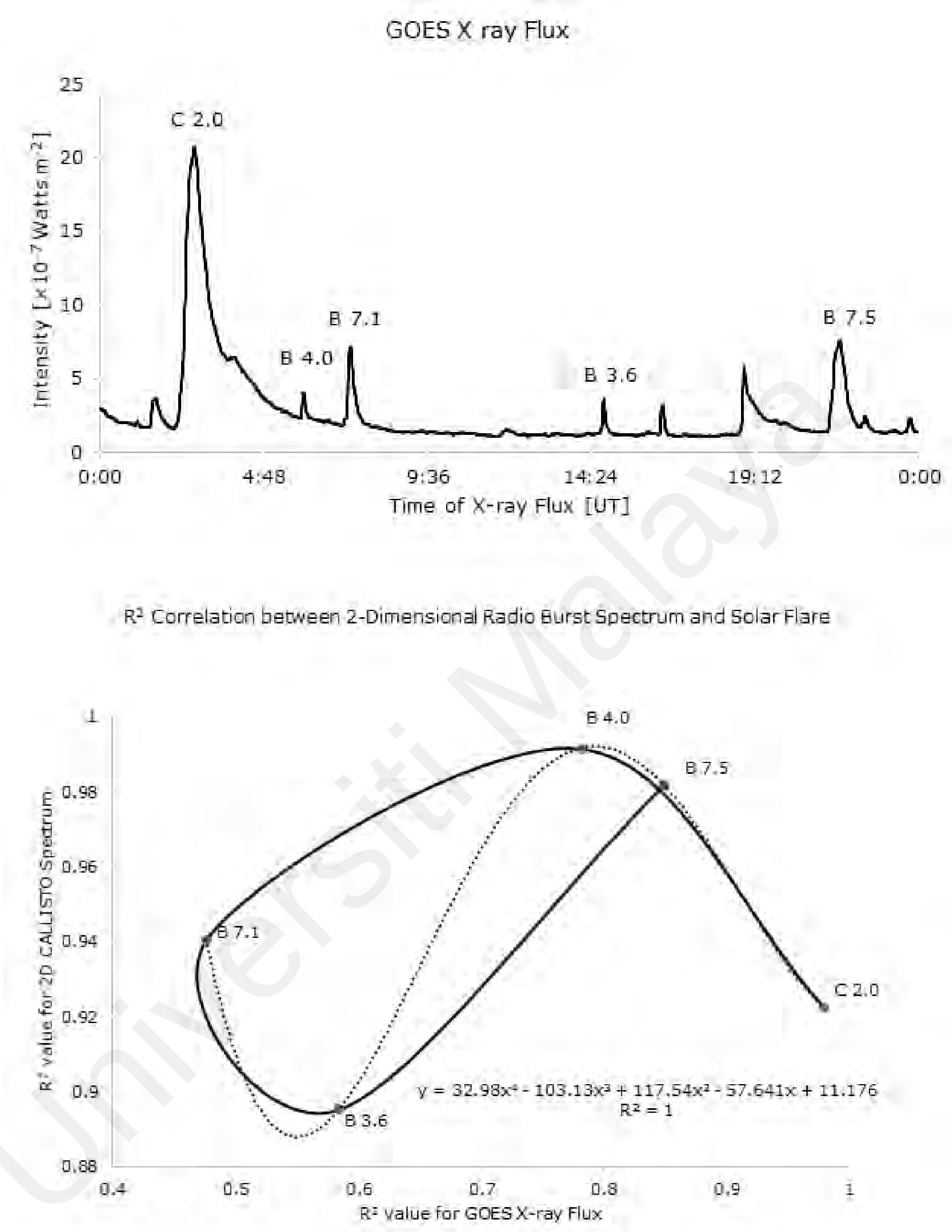

Figure 4.10: Timeline of GOES x-ray flux on 17th April 2017 with indicated peaks that coincides with solar radio burst type III, and R^2 Correlation between 2-Dimensional Radio Burst Spectrum and Solar Flare.

The range of radio signal data is detectable by HWDA lies between 55 to 65 MHz also falls in CALLISTO range. Two of the technologies (HWDA and CALLISTO) compliments one another both in radio frequency range. On a bigger picture, HWDA provides more focus between the small scale ranges of 55 to 65 MHz while CALLISTO gives the overview of the Solar Radio Burst types. In order to understand the explosive transient Universe, radio observations is required because it leads to the effects of magnetic fields studies and the non-thermal processes (Bowman et al., 2013). This section is required as it provide indirect measurement of the Sun's particle behaviour on a collective phase. This section is a necessary step that need to be taken once HWDA is fully developed and functions at its optimum point. In order to understand HWDA, which can initiate small and more focus range particle behaviour, assuming the broad view of solar events wholly can be studied through solar radio burst event via CALLISTO and solar flare data through GOES. It is clearly proven correlating electromagnetic transients is unlocking substantial new physics (Bowman et al., 2013). This is important especially HWDA is newly constructed technology. The study of solar radio burst type (CALLISTO) and solar flare (GOES) is to get to the bottom of answering HWDA. For low frequency transient radio emission limited observational constraints (Bowman et al., 2013), so the correlation between radio and x-ray flux extends the research of HWDA on entire perspective of solar event by conferring some expected physical parameters. Studying CALLISTO and GOES datas is consider as surveys to cover the unexplored phase space of HWDA.

In pretext, the ionosphere and the magnetosphere are regarded as a cold magnetoplsma. The wave's propagation signifies the comparisons of low frequency plasma with ionic gyrofrequency to high frequency plasma with electronic plasma frequency (Booker & Dyce, 1965). The quartic equation is presenting itself the polynomial order of the Booker quartic equations. The dispersion relation for a magnetoplasma is generalized as the Booker quartic (Budden, 1988).

4.3 HWDA Potential in Solar Radio Burst

Solar Radio Burst itself is a recognized event to be studied. The event shows high prospect in HWDA to acknowledge the instrument in Solar radio astronomy research. Solar Radio Burst Type II is an interesting study in terms of its two emissions and other related coronal dynamics. Notably, the solar radio burst type II has its fundamental emission that lies between 20 and 60 MHz, while the backbone for this harmonic emission is between 60 and 90 MHz (Zucca et al., 2012). At approximately 60 MHz, each emission starts and ended, hence it is a wise assumption to investigate this separation between the emissions. In this research, solar radio burst type II is studied through drift rates and shock speed resulting its solar dynamics.

4.3.1 Bandpass frequency range (at 60 MHz)

The power-law relationships, $f\ (r)= 307.87r^{-3.78} - 0.14$ (Kishore et al., 2016; Gopalswamy et al., 2009) can be used for all solar radio burst type II and manipulating it with Equation (3.4), the value L_n can be estimated. In the bandpass of the antenna, for $f \approx 60$ MHz, the value of n is 4.44×10^7 m^{-3}, and r is approximately 1.54 R_Θ (solar radii), consequently leading L_n from Equation (3.9) (Gopalswamy et al., 2009) equals to -0.203 R_Θ (or -1.41×10^8 m) where the negative value indicates the emission is moving out of the solar surface. By computing L_n, the shock speed, v from Equation (3.8) can be estimated. Table 4.1 shows an estimation of the drift rate, $\frac{df}{dt}$, which is calculated based on a few selected Solar Radio Bursts type II (assuming the starting frequency at 60 MHz at fundamental emission).

Table 4.1: Approximate solar radio burst type II with their respective drift rates and shock speed at 60 MHz fundamental emission.

$\frac{df}{dt}$(MHzs^{-1})	v (ms^{-1})
0.0005	2.350 x 10^3
3.2	1.504 x 10^7

Table 4.1 show the drift rate of an example of a low slow drift (or minimum), 0.0005 MHzs^{-1} and a high slow drift (or maximum), 3.2 MHzs^{-1} for solar radio burst type II with their respective shock speeds of 2.350 x 10^3 ms^{-1} and 1.504 x 10^7 ms^{-1}. The drift rate 3.2 MHzs^{-1} is obtained from a study by Batubara et al. (2017), which indicate a high magnitude for slow drift burst. While, the drift rate 0.0005 MHzs^{-1} can be regarded as the lowest drift rate.

4.3.2 Estimation using CALLISTO

Energetic Sun's eruption emits solar radio burst type II usually is related with CME in association of a flare event. Blast wave and mass acceleration produce from solar flare initiated solar radio burst. In calculation from previous research, the density enhancement factor is estimated by inserting an integer as its value varying from 1 to 5 (Doddamani et al., 2014). Figure 4.11 show the spectrogram at Greenland dated 3rd April 2017 at approximately 14:26UT to 14:44UT. With linear approach, the Solar Radio Burst type II shows drift rates of -0.0541 MHzs^{-1}, and -0.0874 MHzs^{-1}. Figure 4.12 show the spectrogram at Greenland dated 18th April 2017 at approximately 19:48 UT to 20:04 UT. With the drift rates of -0.0309 MHzs^{-1}, and -0.0438 MHzs^{-1}. Figure 4.13 show the spectrogram at Greenland dated 2nd September 2017 at approximately 15:34 UT to 15:48 UT with the drift rates of -0.0565 MHzs^{-1}, and -0.1142 MHzs^{-1}. Figure 4.14 show the spectrogram at Greenland dated 6th September 2017 at approximately 12:02 UT to 12:22 UT with the drift rates of -0.0765 MHzs^{-1}, and -0.1425 MHzs^{-1}. Figure 4.15 show the spectrogram at Blein (in Switzerland) dated 12th

September 2017 at approximately 07:30 UT to 07:42 UT with the drift rates of -0.0689 $MHzs^{-1}$, and -0.0903 $MHzs^{-1}$. The dashed white line indicated drift rates with linear approach. The solid white arrow points the first drift rate that coincides at 60MHz. The negative drift rate values indicating the radio emission is leaving the Sun surface, indicating the particles are moving away from the Sun. As such, particles movement occurs randomly. Although collectively, the CALLISTO detect the bigger picture of Solar Radio Burst but the small scale of the particles true nature can't be detected. A positive drift rate can only be calculated if a pattern inside a spectrogram indicating it is moving downward, hence towards the Sun surface. For this matter, a researcher cannot simply imply the enlarge image features since the resolution would be totally out of focus. Therefore, the particle movement can only be seen in a smaller scale range, hence the making of HWDA technology.

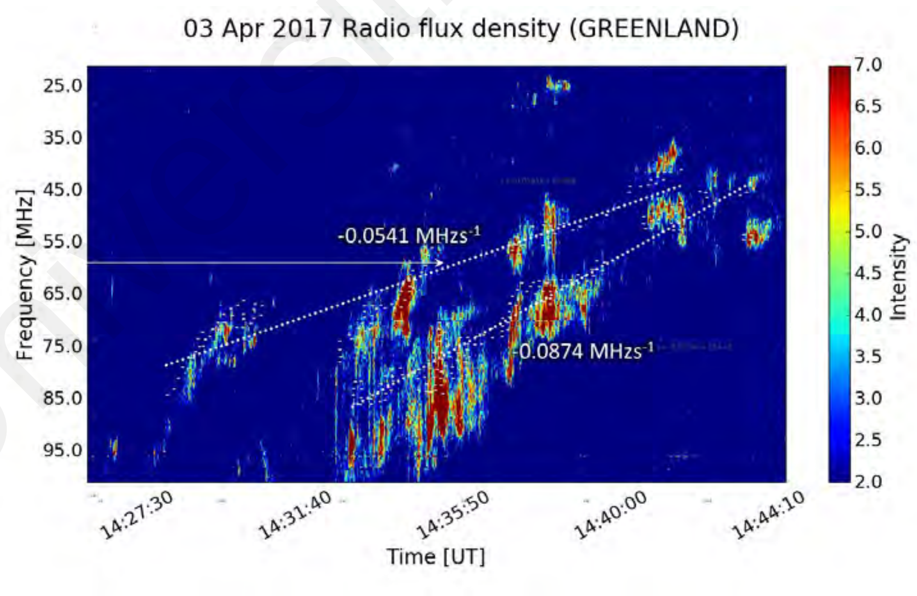

Figure 4.11: The spectrogram at Greenland dated 3rd April 2017 at approximately 14:26UT to 14:44UT. With linear approach indicated in white dashed line, the Solar Radio Burst type II shows drift rates of -0.0541 $MHzs^{-1}$, and -0.0874 $MHzs^{-1}$. The white solid arrow indicated the drift rate at 60 MHz coincides at -0.0541 $MHzs^{-1}$.

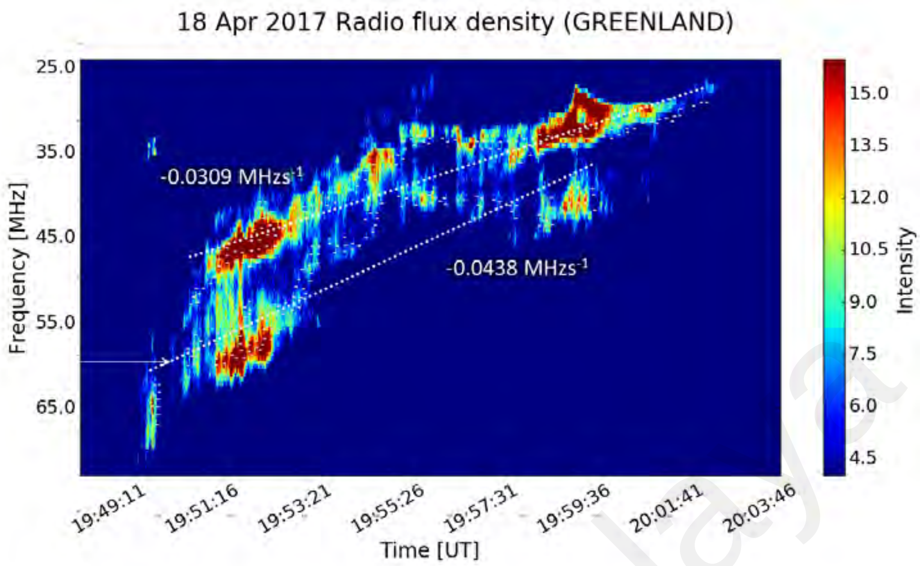

Figure 4.12: The spectrogram at Greenland dated 18th April 2017 at approximately 19:48 UT to 20:04 UT. With linear approach indicated in white dashed line, the Solar Radio Burst type II shows drift rates of -0.0309 MHzs^{-1}, and -0.0438 MHzs^{-1}. The white solid arrow indicated the drift rate at 60 MHz coincides at -0.0438 MHzs^{-1}.

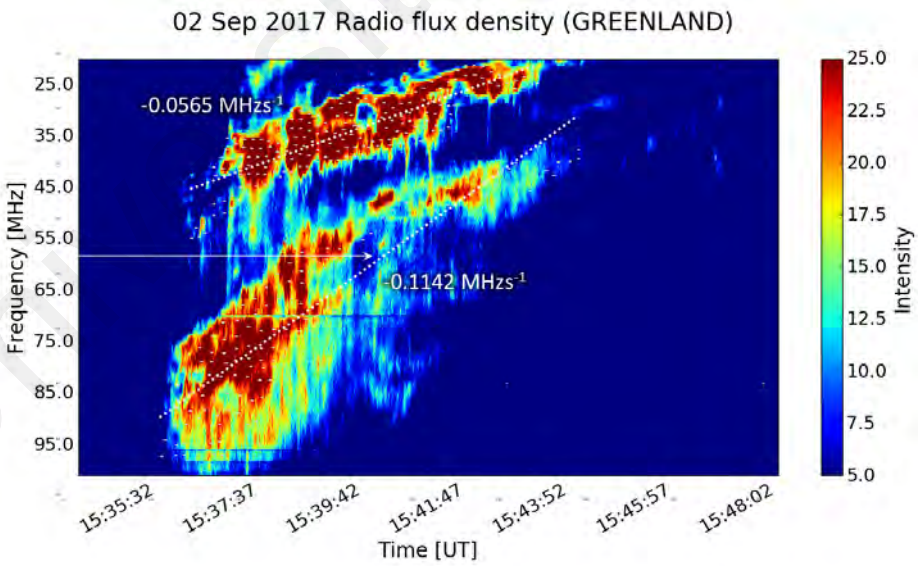

Figure 4.13: The spectrogram at Greenland dated 2nd September 2017 at approximately 15:34 UT to 15:48 UT. With linear approach indicated in white dashed line, the Solar Radio Burst type II shows drift rates of -0.0565 MHzs^{-1}, and -0.1142 MHzs^{-1}. The white solid arrow indicated the drift rate at 60 MHz coincides at -0.1142 MHzs^{-1}.

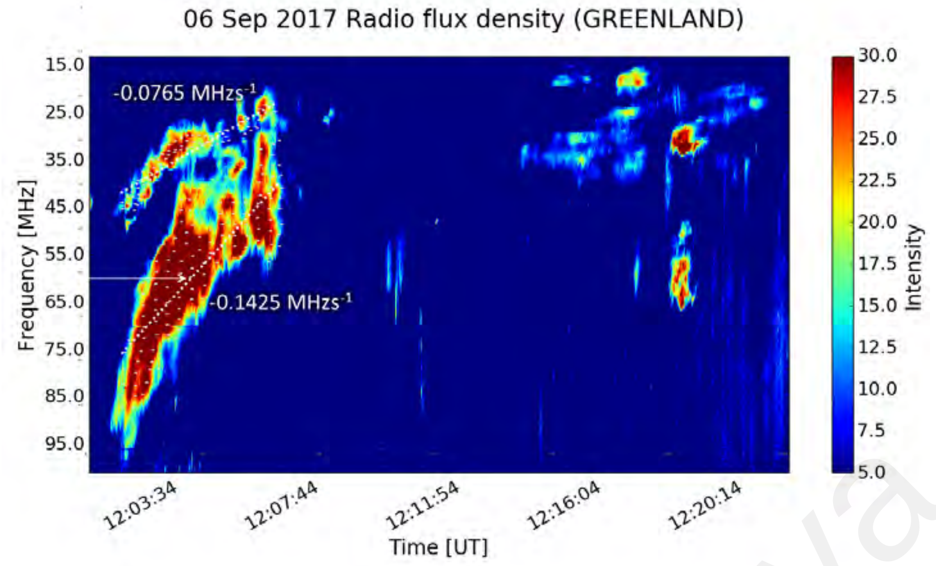

Figure 4.14: The spectrogram at Greenland dated 6th September 2017 at approximately 12:02 UT to 12:22 UT. With linear approach indicated in white dashed line, the Solar Radio Burst type II shows drift rates of -0.0765 MHzs^{-1}, and -0.1425 MHzs^{-1}. The white solid arrow indicated the drift rate at 60 MHz coincides at -0.1425 MHzs^{-1}.

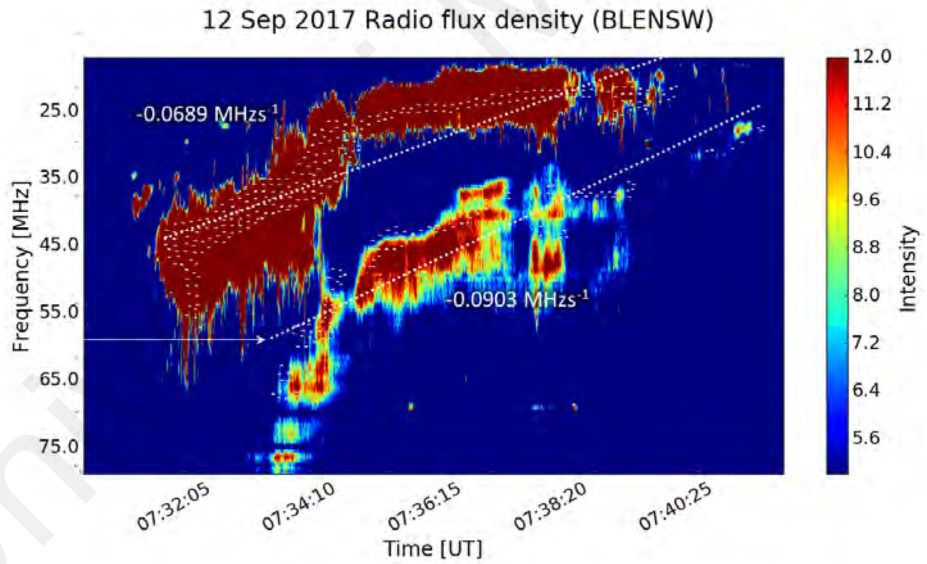

Figure 4.15 : The spectrogram at Blein (in Switzerland) dated 12th September 2017 at approximately 07:30 UT to 07:42 UT. With linear approach indicated in white dashed line, the Solar Radio Burst type II shows drift rates of -0.0689 MHzs^{-1}, and -0.0903 MHzs^{-1}. The white solid arrow indicated the drift rate at 60 MHz coincides at -0.0903 MHzs^{-1}.

Figure 4.15 at Blein (in Switzerland) dated 12th September 2017 at approximately 07:30 UT to 07:42 UT coincides with HWDA observation time window but no available data were recorded. The newly constructed instrument were proven reliable on 17th April 2017 when it successfully recorded radio signal with solar radio burst type III detection. Due to unforeseen technical uncertainty, no data were recorded on 12th September 2017. At the moment the newly constructed technology (HWDA) is still at developing stage where readings are not available daily, and regular troubleshooting problems involving the receivers is making the data capture irregularly unavailable.

A correlation graph has been made for the collected solar radio burst Type II(s). Solar radio burst type II events dated 3rd April 2017, 18th April 2017, 2nd September 2017, 6th September 2017 and 12th September 2017 has been chosen in this correlation study. Each of the date coincides at 60MHz for the drift rate of -0.0541 $MHzs^{-1}$, -0.0438 $MHzs^{-1}$, -0.1142 $MHzs^{-1}$, -0.1425 $MHzs^{-1}$, and -0.0903 $MHzs^{-1}$ respectively. Calculated shock speed, v are 255025.8 ms^{-1}, 206471.9 ms^{-1}, 538335.4 ms^{-1}, 671740.8 ms^{-1}, and 425671.5 ms^{-1} respectively. From the McConell relation, Equation (3.10), a graph of $\frac{df}{dt}$ against $\frac{v}{c}$ is computed.

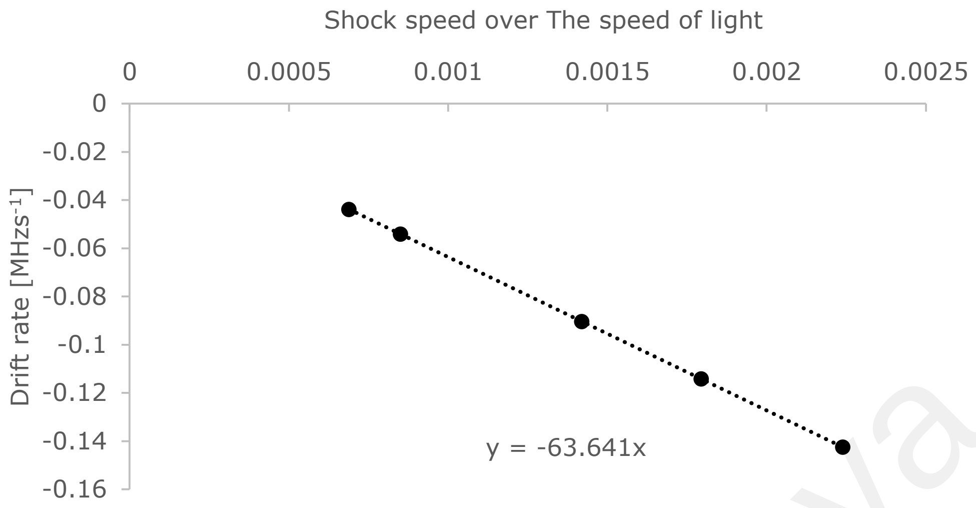

Figure 4.16: Graph of *df/dt* against *v/c* is computed through McConell relation manipulation.

From Figure 4.16, the gradient of -63.641 MHzs^{-1} equals to -(8.7 × 10^{-2}) × f_{obs} $\ln(\frac{0.54\, f\text{obs}}{S\sqrt{M}})^2$. By computing the gradient, with the harmonic number, $S = 2$ since all the events occurred at harmonic emission and the observed frequency is 60 MHz, the density enhancement factor, M is 0.24. Usually solar activity level is taken account according to the density enhancement factor and it doesn't necessarily need to be an integer. However, sometimes quite Sun may generate flare and solar radio burst. For this reason, there are no exact true guidance of indicating the value as high or low. The value can still be validated for these particular solar radio burst Type II events.

CHAPTER 5: DISCUSSION

In this chapter, each section discussed the objectives and its results accordingly. Section 5.1, discussed about the first light of HWDA. Section 5.2, discussed about the association between solar radio burst and solar flare. Section 5.3, discussed the potential of HWDA in investigating solar radio burst type II.

5.1 HWDA First Light

Solar radio burst type II and III have been known to associate with auroral and cosmic rays ejections respectively (Thompson, 1959). Nevertheless, this two solar radio burst can be related. Previously, there were confusion between type II and III spectral classification (Dodson & Hedeman, 1958). This probably because solar radio burst type III often precedes solar radio burst type II (Thompson, 1959). The study of solar radio burst type III is equally important as solar radio burst type II. New technology is being built globally to study their importance especially their relationship with the hazardous CME.A detected solar radio burst type III by HWDA as shown in the green trendline in Figure 4.1 coincides with CALLISTO as shown in Figure 4.3. The fast drift or the almost vertical line of the dynamic spectrum are caused by the high accelerated electron beam (Gopalswamy, 2011). Solar radio burst type III is prominent at low frequency (Gopalswamy, 2011) making it highly detectable in the range of the HWDA.

The alternating signs of the drift rates signifies the propagation of plasma through the small range of 55 to 65 MHz HWDA detection. In solar radio burst type III, the radio waves via the electron beam travel from high to low frequency accordingly the lower frequency radio emission reach the observer later than higher frequency causing the drift rate to be negative. Usually, the source of solar radio burst type III are electron beams moving with constant velocity for a long journey away from the Sun, and even farther than the Earth orbit. The drift rate depends on the coronal density. Commonly, positive drift rates indicate the electron beams being generated by Solar Radio Burst type III is moving towards the Sun while negative is vice versa. The positive drift rate is related to the motion of radio source in the direction of increasing density. Insisting the alternating drift rate signs came from the same electron beams generated by the same normal solar radio burst type III is connected through plasma properties in terms of electron beams. The fact of radio emission, it could be slightly lower than the speed of light and similar to the speed of electron. The group velocity of solar radio burst type III emission with lower plasma temperature is lower than of the electron velocity resulting the radio waves travel behind the electrons. This is causing the lower frequency emission reaches the observer earlier than of higher frequencies and hence, the positive drift rates occurred (Melnik et al., 2015).

From the preliminary results HWDA, the interpretation of graph in Figure 4.2 should emphasize on the alternating signs of the drift rate because the magnitude is showing point gradients not describing the burst collectively. Although the HWDA is at its new stage of development, but it can offer a potential study with the alternating signs in drift rates. That eventually tells the behaviour of solar radio burst can be studied through the movement of electron in its radio emission. In rare occurrence, solar radio burst type III is observed for normal, fast and the alternating sign of drift rates in decameter band or high frequency range (HF=3 - 30 MHz) due to plasma properties which electron propagates (Melnik et al., 2015). Meanwhile, the alternating signs is common for decimetre band or ultra-high frequency (UHF=300 MHz – 3 GHz) due to simultaneous propagation of electron beams toward and away from the Sun (Melnik et al., 2015). HWDA has given the potential to observe the alternating drift rates can also be observed at very high frequency (VHF = 30 - 300 MHz).

Solar Radio Burst Type III is a really broad range radio spectrum that covers 10 kHz to 1 GHz. In the modern world where telecommunication technologies operates within that frequency could be disastrous if large interference of the magnetic energy coincides with the earth's magnetic field. Most of telecommunication technologies on earth is to be exact at VHF range is within that range. Media for VHF TV Broadcasting, FM Radio, Ship & Aircraft Communication, and Police & Fire Radio Systems will be greatly affected. According to Malaysian Communications and Multimedia Commission (MCMC), Malaysia will suffer interfere signals of VHF TV broadcasting that basically covers RTM Channels. Malaysian government been using the Channels to communicate with public citizen in Malaysia. The channels act as one of medium between the commoners and the governments, especially in spreading news. VHF range is an important in spreading news especially in the mist of global pandemic terror. It is necessary to study the origin that are causing to interfere with the range. Studying Solar Radio Burst is a secondary study of the VHF range. Hence, studying Solar Radio Type III is an important course as it indirectly affecting the modern world.

The alternating drift rate signs suggest the plasma temperature is intermittently constant. This might be best explained with non-thermal processes. Knowingly, the observation on thermal and non-thermal effects is very difficult to distinguish alone on the propagation of electron beams and other processes (Fan & Fisher, 2012). The term non-thermal plasma itself refers to plasma is not in thermodynamic equilibrium. Here, we ought to state the energy of the electron beam is greater than the plasma thermal energy making the temperature of the electron beam is higher than the neutral plasma. In the Coulomb field of thermodynamic equilibrium particles, the kinetic energy of non-thermal electron drops when it crosses a collisional plasma. Consequently, it will heat up the surroundings target plasma as it stops the fast electrons (Aschwanden, 2006).

The intermittently plasma temperature is also resolving and suggesting the coronal heating paradox. If direct heated magnetic loops happen at the corona, the temperature will increase within the coronal loop when the heating rate surpasses the cooling rate. Utmost heating is required in active regions and the quiet-Sun enclosed in magnetic field structures. Uneven heating can occur with unsolved over watched cadence, however the average excess heating rate can deliver a systematic temperature increment. For nonflared conditions, the structural photospheric arbitrary movement is driven by subphotospheric convection (Aschwanden et al., 2007). The unexplainable fluctuating of temperature as it progresses from the photosphere to the corona is clearly breaking the fundamental of physics about temperature. If the Sun were to compare to a metal ball and the heat came from the core the increasing temperature as heat moves will remain unsolved. Until now, magnetic reconnection is considered as prime energy release in unravel coronal heating (Aschwanden et al., 2007).

The time difference of solar radio burst in HWDA and CALLISTO may be due to transient of radio emission. Radio transient may vary from few seconds to few days of time range caused by explosive objects or events which is the frontier investigation in astrophysics (Bowman et al., 2013). In the solar system, Jupiter is a giant gas planet that produces unknown magnetic field strength by cyclotron maser processes in its magnetosphere with the prediction to emit between 10 and 200 MHz. So far, there have not known searches included radio transient with radio telescopes that have firm results as it is difficult to interpret, due to poor research investigation (Bowman et al., 2013). However, HWDA did show a potential by detecting the solar radio burst, the first light result offers possibilities in the instrument future outcome.

The ways of determining drift rate in solar radio burst are subjective. From the negative drift rate values obtained in Figure 4.4, the drift rate is calculated as each represent streams that collectively shows the electron beam are moving away from the sun. The linear regression gradient in calculating drift rates doesn't describe the best fit of linear function between the spectrogram axes of Solar Radio Burst Type III. This is simply a close approximation in determining the value of the frequency drift (or drift rates) in proving the observation of Solar Radio Burst Type III. Collectively in stream the electrons propagations set up different plasma collision. Apart from that, it is hard to identify the electron (plasma) propagation. From these, the lack of spatial focus has shown its incapacity of detecting the movement of electron in solar radio burst. The system is at the state of having detection to show its capability of detecting solar radio burst to verify its feasibility in studying solar radio burst type II. In the near future, this novel research leads to two countries (Malaysia and China) interferometry of between UM and YNAO will solve the spatial resolution.

5.2 The Correlation of Solar Radio Burst and Solar Flare

Magnetic reconnection caused strayed sun particles travels near to speed of light, including other factors like wave-particle interaction (Howell, 2019). The concentrated energy of highly conducting plasma by magnetic reconnection somehow accelerate the strayed particles. For instance, the events such as the solar wind where the strayed particles of charged particles is constantly emitted into the interplanetary spaces. A complex magnetic field by linking twirl of high current flows is created through the highly energetic particles surrounding the Sun which drives the currents to move the charged particles. The ever growing interlinking swirl of particles cause magnetic field complexity in and out the Sun. This in turn initiated a sudden change in the Sun's topology. The release of energy may cause events to occur above the sun surface (Gaughan, 2019).

In theory, wave-particle interaction can be seen through the nature of Solar radio burst having its own speed travelling in radio wave. In layman's point of view, the particles are speeding in its medium (radio wave) while travelling in the speed of light. The natural occurring of wave particle interaction is happening all over the universe. Researchers globally has been flourished with theories to protect delicate space craft and satellite materials since the interaction may cause system malfunctions. Experimentally the particles is being cryptically observed by researchers all over the world (Howell, 2019).

The approximation of an ideal MHD is always used to describe solar flares as it occurs in a complex magnetized plasma environment through simulations to explore the properties of flares, but in practice this aspect is understated in physics (Hudson et al., 2011). In multiple regression, R^2 also known as the coefficient of multiple determination is a statistical approach of data points behaviour towards its best fitted line.

Solving the Booker quartic is simple as it describes the modes when the wave frequency is well above the plasma frequency, which it is for most cases in transionospheric propagation (Barnes, 1997). But this not the case in reflective propagation, analysis might be due to the estimation of the phase changes by including the rotation of the electric fields of the characteristic modes, since the existence the Booker quartic in ionospheric regions and the polarization of the modes is changing very rapidly (Barnes, 1997). Observed Faraday rotation is affected by complex electric field vector rotation (Barnes, 1997). Indirectly, the function (quartic equation) utterly describing Faraday rotation. Faraday rotation is the rotation of polarization plane of an electromagnetic wave after propagating through a birefringent medium in free space (Barnes, 1997). Ultimately, the correlation between solar radio burst and solar flare is unfolding the manner of electromagnetic waves is disturbed through the events of Faraday rotation.

5.3 Solar Radio Burst Type II in HWDA

The generation of solar radio burst type II has been speculate between flare and CME that leads to two mechanisms in the formation of shockwaves, which is the 'piston mechanism' and the 'pressure mechanism' respectively (Vršnak & Lulić, 2000). In the 'pressure mechanism', a sudden pressure pulse produces MHD blast waves which later transforms to shock waves (Vršnak & Lulić, 2000). MHD waves describes the movement of plasma in solar radio burst type II using the magnetic reconnection equations. Magnetic reconnection is a region where straight magnetic field lines breaks, changing their geometric and spatial relations, before it reconnects back within that region (Schnack, 2009). The magnetic reconnection equations in Chapter 2 is a relation that gives an idea how an electromagnetic wave act as plasma particle especially in terms describing solar burst motion. At a really large conductivity in an ideal MHD, the diffusion term approaches zero. The magnetic field against time then shows the convection term of the magnetic reconnection equation which clearly explains the movement of plasma in terms of magnetic field. It describes the relationship between solar radio burst type II and MHD. This relation postulates the origin of solar radio burst type II through pressure pulse mechanism which produce MHD blast waves (Vršnak & Lulić, 2000). In laymen's term, diffusion defines the spreading of a certain or constituent part of a component travel in a medium, while convection defines the movement within a fluid that results in heat transference, which in our case energy transference in the form of electromagnetic wave. In other words, assumption on calculating the velocity will become less complicated.

Kilometric type II is associated with CMEs that able to drive shocks only when it reaches far into the interplanetary medium (Winter & Ledbetter, 2015). Note that the solar radio bursts are chosen to estimate the drift rates and shock speed, if it occurs at 60MHz fundamental emission. As a reminder, this is the center frequency band of the newly-constructed HWDA array.

The Zimovets et al. (2012) illustration describes the harmonic emission of solar radio burst type II. In general, the origin of the frequency band splitting is still not yet fully understood. This problem mainly arises from the lack of spatially resolved observations on solar radio burst type II sources (Zimovets et al., 2012). Although the spectrogram from CALLISTO is a good approach in estimating physical parameter such as shock speed for solar radio burst type II, but a small scale observation by HWDA gives a better resolution, in terms of intensity curves between the fundamental and harmonic emission gap. The Sun activity is indicated using the density enhancement factor. However, there is no true value suggesting in determining the activity during quiet or active Sun (Doddamani et al., 2014). In this research the value is estimated by correlating five solar radio burst type II occurred in 2017.

The level of solar activity is usually determined by the density enhancement factor but sometimes this is not necessarily essential. There is no true guide of indicating the level of solar activity, since the quiet Sun may generate flare and solar radio burst but the value can still be validated for these particular solar radio burst Type II events. The use of CALLISTO will aid the detection capability of the HWDA array in terms of confirmation of any future detection. Historically, the ETH Zürich has designed a Compact Astronomical Low-Cost Low-frequency Instrument for Spectroscopy and Transportable Observatory (CALLISTO) that in principal operates at the frequency of 45 MHz until 870 MHz with 15 minutes interval. The spectrograms represent a 3D graph where the color contour between orange and blue shows the flux intensity of the radio emission. The instruments are installed in many locations all over the world such that there is a network to monitor the meter and decameter bands (Zucca et al., 2012).

There are few known radio monitoring technologies that were also a guide in studying solar radio burst using HWDA. For example, *Chinese Spectral Radio Heliograph* (CSRH) and *Murchison Widefield Array* (MWA). CSRH was constructed to study the solar radio environment covering wavelength from decimetre to centimeter. This is equivalent to the range between 0.4 GHz and 15 GHz. The main science aim of CSRH is to study the coronal dynamics. It is also used to study the fundamentals problems of energy release, particle acceleration and particle transport from the Sun (Yan et al., 2009). The MWA array is located in Western Australia and specifically designed to explore at a range between 80 MHz until 300 MHz. Other than the use in studying the cosmic web, radio relics, galaxy clusters, Faraday tomography, magnetic fields, the Magellanic Clouds, cosmic ray mapping, galactic supernova remnants and radio recombination lines (Bowman et al., 2013), MWA can also be used to study the solar radio signals (Oberoi et al., 2017).

Figure 5.1 shows technical comparisons of spectrometers around the world that have capabilities of detecting different types of solar radio bursts. The comparison was made to show that all these instruments are needed for a comprehensive study of the solar radio bursts. With the range of 55 to 65 MHz, the HWDA coincides with solar radio burst type II, III, and IV. At 45 to 870 MHz, the CALLISTO coincides with all solar radio burst namely type I, II, III, IV, and V. At 0.4 to 15 GHz, CSRH coincides solar radio burst type III and IV. At 80 to 300 MHz the MWA also coincides with all types of solar radio burst.

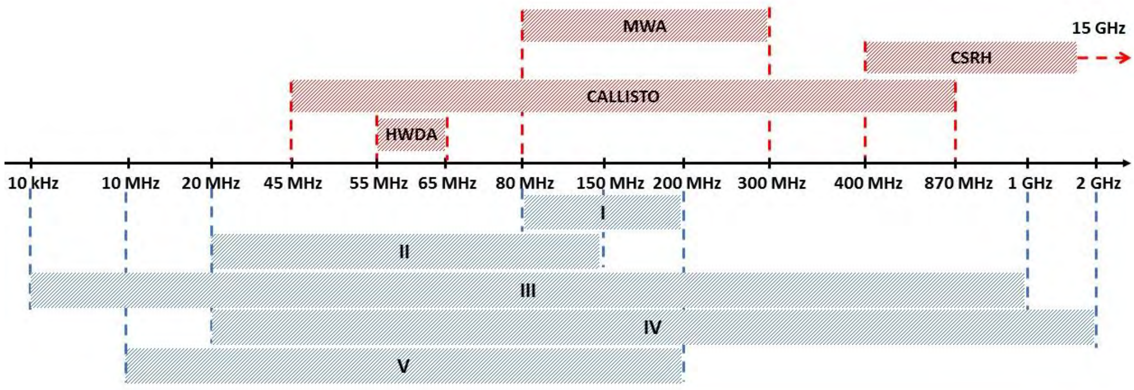

Figure 5.1: Frequency range showing all types of solar radio burst collectively and related radio telescope.

CHAPTER 6: CONCLUSION

In this chapter, each section stated the conclusion according to the objectives. Section 6.1, concludes the first objective, to show the ability of detecting solar radio burst using the half wave dipole antenna. Section 6.2, concludes the second objective, to identify the capability of HWDA by studying the relationship between solar radio burst and solar flare. Section 6.3, concludes the last objective, to discover the potential of HWDA in investigating solar radio burst through its distinct emissions, shock speed and drift rate.

6.1 HWDA Solar radio Burst detection

A radio signal was present in the HWDA signal processing software on the 17th April 2017. There is one significant pattern with peaks at approximately 10:47:04 a.m. (at 02:47:04 UT for 63.6 MHz frequency), 10:47:14 a.m. (02:47:14 UT, 63.4 MHz) and 10:47:25 a.m. (02:47:25 UT, 63.8 MHz). Through linear approach between the trendlines, the drift is calculated as 0.01 MHzs^{-1} and -0.02 MHzs^{-1}. Emphasizing the alternating drift sign indicates temperature change postulating the existence of non-thermal processes and coronal heating. The detection was confirmed Solar radio burst type III by the CALLISTO spectrograms at 17th April 2017 at approximately 02:50:37 UT to 02:51:00 UT indicating 2.59 MHzs^{-1}, -4.55 MHzs^{-1}, and -1.91 MHzs^{-1} Fast drifts moving away from the Sun. With three minutes difference, the small-scale frequency range HWDA properties shows solar radio burst detection.

6.2 HWDA Science in Solar Radio Burst and Solar Flare Association.

The 2D spectrum constructed from a CALLISTO spectrum at Almaty, Kazakhstan of a solar radio burst type III at 59.75 MHz on 17th April 2017 at 02:50 UT were chosen because it has the highest intensity for the radio spectral spectrogram. The GOES X-ray flux shows class C 2.0 solar flare maxes at 02:47 UT, while the 2D spectrum have the highest intensity at 02:50:49 UT. As mentioned by Tandberg-Hanssen (1957), the correlation is positive when Solar Radio Burst happens within 10 minutes range of the solar flare occurrence. Both events show a ratio of R^2 value from GOES X-ray Flux to the 2D spectrum at approximately 0.94. This indicates a strong correlation relationship between the solar radio burst and solar flare of that particular date. This indicates a strong correlation relationship between the solar radio burst and solar flare of that particular date. The R^2 Correlation between 2-Dimensional Radio Burst Spectrum for solar radio burst type III detected by CALLISTO and Solar Flare on 17 April 2017 (with class C 2.0, B4.0, B 7.1, B 3.6, and B 7.5) indicate a quartic function that confirms Faraday rotation in altering and disturbing electromagnetic waves in the ionosphere.

6.3 HWDA in Solar Radio Burst Criterion.

The potential of HWDA in Solar radio Burst dynamics is investigated. Previous research indicates that there is a lack of spatial resolution of solar radio burst type II study. Gopalswamy model, as mentioned in Chapter 3 is a good approximation with a correlation coefficient of 0.56 between the starting frequency, *f*, and CME height, *r*. The range between 55 to 65 MHz will give a higher spatial resolution of the gap between the fundamental and harmonic emission in solar radio burst type II detections. The Zimovets et al. (2012) model explains the band split that occurs at the harmonic emission. Gopalswamy power law and the electron density were used to estimate the density scale height, L_n. At 60 MHz, the L_n was estimated to be -1.41 x 10^8 m and this can be used to calculate the shock speed at that frequency. The calculated shock speeds of 2.350 x 10^3 ms^{-1} and 1.504 x 10^7 ms^{-1} at the starting frequency of 60 MHz using low 0.0005 $MHzs^{-1}$ and high drift rates, 3.2 $MHzs^{-1}$ respectively.

Solar activity can be determined using the density enhancement factor. A correlation of five solar radio burst type II events 3rd April 2017 (drift rate of -0.0541 MHzs^{-1} and shock speed of 255025.8 ms^{-1}), 18th April 2017 (-0.0438 MHzs^{-1}, 206471.9 ms^{-1}), 2nd September 2017 (-0.1142 MHzs^{-1}, 538335.4 ms^{-1}), 6th September 2017 (-0.1425 MHzs^{-1}, 671740.8 ms^{-1}) and 12th September 2017 (-0.0903 MHzs^{-1}, 425671.5 ms^{-1}) that coincides at 60 MHz computes a density enhancement factor of 0.24. As an addition, an ideal criterion for selecting solar radio burst type II is that the radio emission must have indication of a distinguished fundamental and harmonic bands. In other words, the two bands must have well-defined edges to allow the frequency to be determined up to 1 MHz; and the duration of the frequency band splitting must be sufficient to allow the drift-rate to be at most 10 percent accuracy (Smerd et al., 1975) which is then being compared to CALLISTO.

In general, solar radio burst, CME and solar flares are events of solar activities that possess their own significant magnetic properties. They can cause disturbance towards earth's magnetosphere and that in return can cause satellite communication interference, shortwave radio fades, blackouts on satellite, compass alignment error, electrical power blackouts, communication landlines and equipment damage. Indirectly, solar activities affect humans' life in needs and health. This is why understanding solar radio bursts presents as much importance as studying the CME and solar flares. Advanced electronic system that arise from modern society technological dependence making the Earth vulnerable to electromagnetic disturbance. Large-scale electric field during electromagnetic disturbance resulting voltage and current overloads that may interfere with power grids affecting the current modern lifestyles (White, 2007). The solar events induced disturbance that may affect the Earth surrounding (Klein et al., 2018). Generically, Space Weather is the condition of solar wind inside the Earth surrounding. Including the speed, density, energetic particle levels, magnetic field strength and its orientation that origins from solar events. The magnetosphere and Earth's atmosphere shields us from harmful disaster (White, 2007). It is obvious, the study of solar radio burst pinned points to the origin of Space Weather especially in understanding the physical processes involved.

REFERENCES

Aschwanden, M. J., & Benz, A. O. (1995). Chromospheric evaporation and decimetric radio emission in solar flares. *The Astrophysical Journal*, *438*, 997-1012.

Aschwanden, M. (2006). *Physics of the solar corona: An introduction with problems and solutions*. Chichester, UK: Springer Science & Business Media.

Aschwanden, M. J., Winebarger, A., Tsiklauri, D., & Peter, H. (2007). The coronal heating paradox. *The Astrophysical Journal*, *659*(2), 1673-1681.

Barnes, R. I. (1997). Faraday rotation in a cold, inhomogeneous magnetoplasma: A numerical comparison of ray and full wave analyses. *Radio Science*, *32*(4), 1523-1532.

Batubara, M., Manik, T., Suryana, R., Lathif, M., Sitompul, P., Zamzam, M., & Mumtahana, F. (2017, March). Frequency drift rate investigation of solar radio burst type ii due to coronal mass ejections occurrence on 4th November 2015 captured by CALLISTO at Sumedang-Indonesia. In *IOP Conference Series: Materials Science and Engineering* (Vol. 180, No. 1, p. 012048). IOP Publishing.

Behlke, R. (2001). Published Diploma Thesis: Solar Radio Bursts and Low Frequency Emissions from Space. *IRF Scientific Report 275.* Retrieved on 16 May 2016 from http://urn.kb.se/resolve?urn=urn:nbn:se:uu:diva-25427

Benz, A. O. (2009). 4.1. 2.8 Radio bursts of the non-thermal sun. In *Solar System* (pp. 189-203). Berlin: Springer.

Bhatnagar, A., & Livingston, W. C. (2005). *Fundamentals of solar astronomy* (Vol. 6). New Jersey: World Scientific.

Booker, H. G., & Dyce, R. B. (1965). Dispersion of waves in a cold magnetoplasma from hydromagnetic to whistler frequencies. *Radio Science*, *69(4)*, 463-492.

Bowman, J.D., Cairns, I., Kaplan, D.L., Murphy, T., Oberoi, D., Staveley-Smith, L., et. al. (2013). Science with the Murchison Widefield Array. *Publications of the astronomical Society of Australia, 30*, E031, 1-28.

Budden, K. G. (1988). *The propagation of radio waves: the theory of radio waves of low power in the ionosphere and magnetosphere*. New York: Cambridge University Press.

Chen, C., Wang, Y., Shen, C., Ye, P., Zhang, J., & Wang, S. (2011). Statistical study of coronal mass ejection source locations: 2. Role of active regions in CME production. *Journal of Geophysical Research: Space Physics*, *116*(A12), 1-15.

Doddamani, V. H., Raveesha, K. H., Subramanian, K. R. (2014). Estimation of coronal magnetic field using multiple Type II radio bursts. *International Journal of Astronomy, 3*(1), 22-29.

Dodson, H. W., & Hedeman, E. R. (1958). Geomagnetic disturbances associated with solar flares with major premaximum bursts at radio frequencies 200 MC/S. *Journal of Geophysical Research*, *63*(1), 77-96.

Eselevich, V. G., Eselevich, M. V., & Zimovets, I. V. (2016). Possible reasons for the frequency splitting of the harmonics of type II solar radio bursts. *Astronomy Reports*, *60*(1), 163-173.

Falco, M., Costa, P., & Romano, P. (2019). Solar flare forecasting using morphological properties of sunspot groups. *Journal of Space Weather and Space Climate*, *9*, A22, 1-9.

Fitzpatrick, R. (2008). Introduction to plasma physics. *The University of Texas at Austin: sn*, 242. Retrieved on 20 May 2014 from http://www.fulviofrisone.com

Fitzpatrick, R. (2014). *Plasma physics: An introduction*. Florida: Crc Press, Taylor & Francis Group.

Fan, Y., & Fisher, G. (Eds.). (2012). *Solar flare magnetic fields and plasmas* (Vol. 277). New York: Springer Science & Business Media.

Gaughan, R. (2019, August 21). *How long for a solar flare to reach earth?* Retrieved on 20 December 2019 from https://sciencing.com/long-solar-flare-reach-earth-3732.html

Gao, G. N., Wang, M., Lin, J., Wu, N., Tan, C. M., Kliem, B., & Su, Y. (2014). Radio observations of the fine structure inside a post-CME current sheet. *Research in Astronomy and Astrophysics*, *14*(7), 843-854.

Gopalswamy, N., Thompson, W. T., Davila, J. M., Kaiser, M. L., Yashiro, S., Mäkelä, P., ... & Howard, R. A. (2009). Relation between type II bursts and CMEs inferred from STEREO observations. *Solar Physics*, *259*(1), 227-254.

Gopalswamy, N. (2011). Coronal mass ejections and solar radio emissions. *Planetary Radio Emissions*, *7*, 325-342.

Gopalswamy, N., Xie, H., Mäkelä, P., Yashiro, S., Akiyama, S., Uddin, W., ... & Mahalakshmi, K. (2013). Height of shock formation in the solar corona inferred from observations of type II radio bursts and coronal mass ejections. *Advances in Space Research*, *51*(11), 1981-1989.

Gopalswamy, N. (2016). History and development of coronal mass ejections as a key player in solar terrestrial relationship. *Geoscience Letters*, *3*(1), 1-18.

Gou, T., Liu, R., Kliem, B., Wang, Y., & Veronig, A. M. (2019). The birth of a coronal mass ejection. *Science Advances*, *5*(3), eaau7004, 1-9.

Howell, E. (2019, May 31). 3 Ways fundamental particles travel (nearly) the speed of light. Retrieved on 20 December 2019 from https://www.space.com/fundam ental-particles-travel-speed-of-light.html

Hudson, H. S., Fletcher, L., Fisher, G. H., Abbett, W. P., & Russell, A. (2011). Momentum distribution in solar flare processes. In *Solar Flare Magnetic Fields and Plasmas* (pp. 77-88). New York: Springer.

Kishore, P., Ramesh, R., Hariharan, K., Kathiravan, C., & Gopalswamy, N. (2016). Constraining the solar coronal magnetic field strength using split-band type ii radio burst observations. *The Astrophysical Journal*, *832*(59), 1-7.

Klein, K. L., Matamoros, C. S., & Zucca, P. (2018). Solar radio bursts as a tool for space weather forecasting. *Comptes Rendus Physique*, *19*(1-2), 36-42.

Kraus, J. D., Marhefka, R. J., & Khan, A. S. (2006). *Antennas and wave propagation*. New Delhi: Tata McGraw-Hill Education.

Kundu, M. R. (1965). *Solar Radio Astronomy. The Radio Astronomy Observatory*. New York: Interscience Publication.

Kuphaldt, T. R. (2007). *Lessons in electronic circuits, volume II – AC, sixth edition. Design science license.* Retrieved on 20 May 2014 from http://hdl.handle.net /20.500.12091/424

Layton, J., & Freudenrich, C., (2000, October 17). How the sun works. Retrieved on 20 May 2014 from http://science.howstuffworks.com/ sun.htm

Marusek, J. A. (2007). Solar storm threat analysis. J. Marusek. Retrieved on 20 May 2014 from https://www.jumpjet.info/Emergency-Preparedness/Disaster-Mitigation/NBC/E M/Solar_Storm_Threat_Analysis.pdf

Melnik, V. N., Brazhenko, A. I., Konovalenko, A. A., Briand, C., Dorovskyy, V. V., Zarka, P., ... & Denis, L. (2015). Decameter type III bursts with changing frequency drift-rate signs. *Solar Physics*, *290*(1), 193-203.

Monstein, C. (2011). Catalog of dynamic electromagnetic spectra. *Physics, Astronomy, Electronics Work Bench*, 1-16.

Oberoi, D., Sharma, R., & Rogers, A. E. (2017). Estimating solar flux density at low radio frequencies using a sky brightness model. *Solar Physics*, *292*(6), 75-93.

Orfanidis, S. J. (2002). *Electromagnetic waves and antennas* (pp. 739-784). New Brunswick, NJ: Rutgers University.

Pekünlü, E. R. (1999). Solar flares. *Turkish Journal of Physics*, *23*(2), 415-424.

Sato, H., Jakowski, N., Berdermann, J., Jiricka, K., Heßelbarth, A., Banys, D., & Wilken, V. (2019). Solar radio burst events on September 6, 2017 and its impact on GNSS signal frequencies. *Space Weather*, *17*(6), 816-826.

Smerd, S. F., Sheridan, K. V., & Stewart, R. T. (1975). Split-band structure in type II radio bursts from the sun. *Astrophysical Letters*, *16*, 23-28.

Schnack, D. D. (2009). *Lectures in magnetohydrodynamics: With an appendix on extended MHD* (Vol. 780). Berlin: Springer-Verlag.

Tandberg-Hanssen, E. (1957). On the correlation between solar flares and radio bursts. *Astrophysica Norvegica*, *6*, 17-25.

Thompson, A. (1959). The correlation of solar radio bursts by magnetic activity andcosmic rays. *Symposium – International Astronomical Union, 9, 210-213.*

Vršnak, B., & Lulić, S. (2000). Formation of coronal MHD shock waves–I. The basic mechanism. *Solar Physics*, *196*(1), 157-180.

White, S. M. (2007). Solar radio bursts and space weather. *Asian Journal of Physics*, *16*, 189-207.

Winter, L. M., & Ledbetter, K. (2015). Type II and Type III radio bursts and their correlation with solar energetic proton events. *The Astrophysical Journal*, *809*(1), 105.

Yan, Y., Zhang, J., Wang, W., Liu, F., Chen, Z., & Ji, G. (2009). The Chinese spectral radioheliograph—CSRH. *Earth, Moon, and Planets*, *104*(1-4), 97-100.

Zimovets, I., Vilmer, N., Chian, A. L., Sharykin, I., & Struminsky, A. (2012). Spatially resolved observations of a split-band coronal type II radio burst. *Astronomy & Astrophysics*, *547*, A6, 1-13.

Zucca, P., Carley, E. P., McCauley, J., Gallagher, P. T., Monstein, C., & McAteer, R. T. J. (2012). Observations of low frequency solar radio bursts from the Rosse solar-terrestrial observatory. *Solar Physics*, *280*(2), 591-602.